Astron. Astrophys. 228, 125–154 (1990)

ASTRONOMY AND ASTROPHYSICS

Radiation driven winds of hot luminous stars

VII. The evolution of massive stars and the morphology of stellar wind spectra

A.W.A. Pauldrach, R.P. Kudritzki, J. Puls, and K. Butler

Institut für Astronomie und Astrophysik der Universität München,
Scheinerstrasse 1, D-8000 München 80, Federal Republic of Germany

Received December 28, 1988; accepted March 17, 1989

Abstract. A grid of wind models along evolutionary tracks of massive O stars is calculated using the improved radiation driven wind theory developed recently by Pauldrach et al. (1986), Pauldrach (1987) and Pauldrach and Herrero (1988). The intention of the present paper is to investigate the change of spectral morphology during the course of stellar evolution. The results show that the improved stellar wind models can describe the significantly different observed behaviour of the profiles of the Si IV line with respect to those of C IV and N V as a function of spectral type and luminosity class. The physical reason for this effect is explained. In addition, a sequence of O VI line profiles is calculated indicating that the theory is able to produce P-Cygni structures down to $T_{\rm eff} \approx 41\,000$ K. Agreement with observations is also found for the computed mass-loss rates and the ratios of calculated terminal wind velocities and escape velocities, even for late O supergiants. For the wind efficiencies, a strong dependence on mass is found, together with a pronounced decrease from main sequence stars to supergiants and a dramatic increase towards LBVs.

Key words: early-type stars – non-LTE – mass loss – winds

1. Introduction

Since the pioneering work of Lucy and Solomon (1970), Castor et al. (1975), and Abbott (1979), who showed that the radiation force is sufficient to initialize and to maintain stellar winds, the theory of radiation driven winds has been continuously improved. Very detailed and complex multi-level NLTE calculations have become available, that include the radiation driven wind hydrodynamics in a self-consistent way. Pauldrach et al. (1986) and Friend and Abbott (1986) were able to calculate wind models which reproduced the observed terminal velocities (v_∞) and mass loss rates ($\dot{M}$). Kudritzki et al. (1987) showed that the low metallicity of the stars in the SMC and LMC can be the explanation of the lower terminal velocities observed. Pauldrach (1987) demonstrated that the observed highly ionized species like N V and O VI can be produced in cool wind models of O stars by correctly treated full multi-level NLTE calculations. Puls (1987) included the important "multi-line effects" of overlapping lines self-consistently. Pauldrach et al. (1988a, b) and Gabler et al. (1988) were able to reproduce the observed wind features of Central Stars of Planetary Nebula. However, in spite of this progress in the theory of radiation driven winds the quantitative analysis of stellar wind lines is still in a very preliminary state, in particular, when compared with the well established tool of analyzing photospheric lines using NLTE model photospheres and line formation calculations. An important test of the reliability of the improved theory is to investigate whether it describes at least the observed systematic changes of spectral morphology as a function of stellar parameters in a suitable way. Such systematic changes of O star wind lines became evident from the work of Walborn and collaborators (Walborn and Panek, 1984a, b, 1985; Walborn and Nichols-Bohlin, 1987; Walborn et al., 1985). In particular, the Si IV resonance doublet exhibits a strong dependence on *luminosity*. The observations indicate the complete absence of stellar wind features in Si IV on the main sequence, but the wind components develop gradually from the intermediate luminosity classes (III) into saturated wind profiles for the supergiants. This sensitivity of the Si IV stellar wind lines on O star luminosity is particularly interesting, since it is in sharp contrast to the behaviour of other P-Cygni profiles. The resonance lines of C IV and N V, for instance, show strong wind structure from the main sequence through to the O supergiant stage.

It is of course crucial for a quantitative stellar wind theory to reproduce not only v_∞ and $\dot{M}$ but also these effects. This requires, however, detailed and very refined NLTE calculations for excitation and ionization in the winds of hot stars, as was recognized recently by Drew (1988). Fortunately, such realistic calculations are now available.

Pauldrach (1987) adopted a cool wind ($T_{\rm W} \approx T_{\rm eff}$) and treated the full multi-level NLTE problem of all relevant elements and ions including electron collisions self-consistently with the radiation driven wind hydrodynamics. He included in total 26 elements, 133 ionization stages, 4000 levels, 10 000 radiative bound-bound transitions in the rate equations and the correct continuous radiation field for the bound-free rates calculated from the spherical transfer equation. Pauldrach and Herrero (1988) modified the computational method by introducing the accelerated lamda iteration, that allows objects close to the

Send offprint requests to: A.W.A. Pauldrach

Eddington-limit to be handled correctly as well. We have now applied calculations of this type on a grid of wind models along evolutionary tracks of massive O stars to investigate whether our models reproduce the change of spectral morphology during stellar evolution in a reasonable way. In this way we obtain self-consistently calculated P-Cygni profiles and dynamical parameters ($v_\infty, \dot{M}$) simultaneously, which can then be compared with the observations and can also be used as input for evolutionary calculations. Moreover, we calculate a grid of line force multiplier parameters in the HR-diagram that can be used for the analytical formulae for v_∞ and $\dot{M}$ as a function of stellar parameters, developed recently by Kudritzki et al. (1988).

The paper is organized as follows: Sect. 2 gives a brief summary of the theoretical concept and describes the grid of models. Sect. 3 discusses the results with respect to spectral morphology, Si IV luminosity dependence and dynamical properties ($v_\infty, \dot{M}$) of the winds. Section 4 gives conclusions and an outlook on future work.

2. The wind model grid and the selected objects for the comparison with observations

The calculations were carried out using the codes recently developed by Pauldrach et al. (1986), Pauldrach (1987), and Pauldrach and Herrero (1988). We briefly repeat the most important points of our procedure.

Based on calculations of the detailed statistical equilibrium for 26 elements in their different ionization stages together with the radiation transfer, line forces are found and parameterized for the hydrodynamic calculations using the force multiplier concept. In doing so the force multiplier parameter triplet (k, α, δ) is not held fixed, as was originally proposed by Abbott (1982), but is allowed to change with depth in the wind (for the final converged model, however, it is possible in most cases to give depth independent mean values that, when used in the hydrodynamic computations yield the mass loss rate and the terminal velocity in good agreement with the depth dependent parameter triplets). Using these depth dependent line forces the hydrodynamic structure is computed by means of the improved theory of radiation driven winds including the finite cone angle effect. As the force multiplier parameters and the continuum's force due to Thomson scattering depend on the density structure, the ionization rate and the velocity field, an iteration cycle is essential for this procedure.

The theory of radiation driven winds is in principle self-consistent and needs only three free parameters: $T_{\rm eff}$, gravity, and radius of the star all defined at a specified optical depth. In addition the chemical composition enters, which is particularly important as soon as deviations from the "solar composition" are encountered. However, at the moment, the theory is still somewhat imperfect so that additional assumptions have to be made:

i) Emergent fluxes of photospheric plane-parallel models are used at the inner radiative boundary condition for the NLTE calculations in the optically thin part of the wind. These fluxes were taken from Kurucz (1979) – details are described by Pauldrach (1987) and Pauldrach and Herrero (1988). In future work "unified model atmospheres", that describe both the photosphere and the wind selfconsistently will have to be used. (A first step towards this aim is described by Gabler et al., 1988).

ii) A constant kinetic temperature in the wind is adopted and is set equal to the effective temperature. This is a restrictive assumption. The recent work by Drew (1988) demonstrates the importance of metal lines cooling in radiative equilibrium leading to temperatures clearly below $T_{\rm eff}$ in the outer wind. However, this result suffers from the very approximate treatment of the NLTE problem. In addition, the role of mechanical heating has still to be investigated. On the other hand the situation is not totally uncertain, since cool wind models with $T(r) \approx T_{\rm eff}$ at least lead roughly to the observed ionic species in the wind, if correct NLTE multi-level calculations are performed (for details, see Pauldrach 1987). Moreover, warm wind models ($T(r) \approx 5T_{\rm eff}$) or corona models ($T(r) \approx 20T_{\rm eff}$) can be ruled out observationally (Lamers et al., 1984; Baade and Lucy, 1987; Pauldrach, 1987). Hence, we have restricted our present calculations to the most simple but not unreasonable case of setting the local electron temperature equal to the effective temperature throughout the wind.

iii) As nearly 4000 energy levels of 133 ionization stages are considered in our NLTE-calculations, we used a simple approximation for all the photoionization cross sections, which is only accurate to within a factor of two (see Pauldrach, 1987). This approximation may result in inaccuracies especially for the weakly populated ionization stages. Additionally, we used solar abundances for all of our calculations. This can lead to the same effect, particularly, for evolved objects like supergiants where recent photospheric NLTE spectroscopy shows that the products of the CN-bicycle can be encountered in the atmosphere (Kudritzki et al., 1987b; Voels et al., 1988).

For quantitative analyses of stellar wind lines of objects with precisely determined stellar parameters these approximations may have a non-negligible effect on the results. However, the purpose of this paper is only a systematic study of the differential changes of spectral lines along evolutionary tracks of massive stars. At the moment, it is not our intention to try to fit the full wind spectrum perfectly for every individual object, although this is our final goal for future work. In this paper we simply want to demonstrate that the theory reproduces the observed general trends in spectral morphology.

We have calculated wind models along the evolutionary tracks of Maeder and Meynet (1987, hereinafter MM), which include mass-loss and overshooting. Figure 1 displays the investigated parameter domain in both the $\log(g)$–$\log(T_{\rm eff})$ diagram (Fig. 1a) and the HR-diagram (Fig. 1b). The different tracks correspond to the evolution of stars of initial mass 120, 85, 60 and 40 $M_\odot$ labelled by A, B, C, and D, respectively. Wind models have been calculated along these tracks self-consistently for the parameters given in Table 1. The increasing arabic numerals for each track represent the evolution towards different luminosity classes in a sequential manner as indicated in Table 1.

For the comparison with the observed spectral morphology we have selected a sample of objects from the high resolution IUE atlas by Walborn et al. (1985) representing the different luminosity classes along the tracks. The position of these objects superimposed on the MM tracks is given in Fig. 1 and Table 2 contains the corresponding stellar parameters. A few comments are necessary with respect to the latter: Two objects (9 Sgr and δ Ori) have been analysed quantitatively by the Boulder group using high resolution, high signal to noise CCD spectra and detailed NLTE model atmosphere techniques (Voels et al., 1988; Voels, priv. comm.). The results of these analyses for $T_{\rm eff}$ and

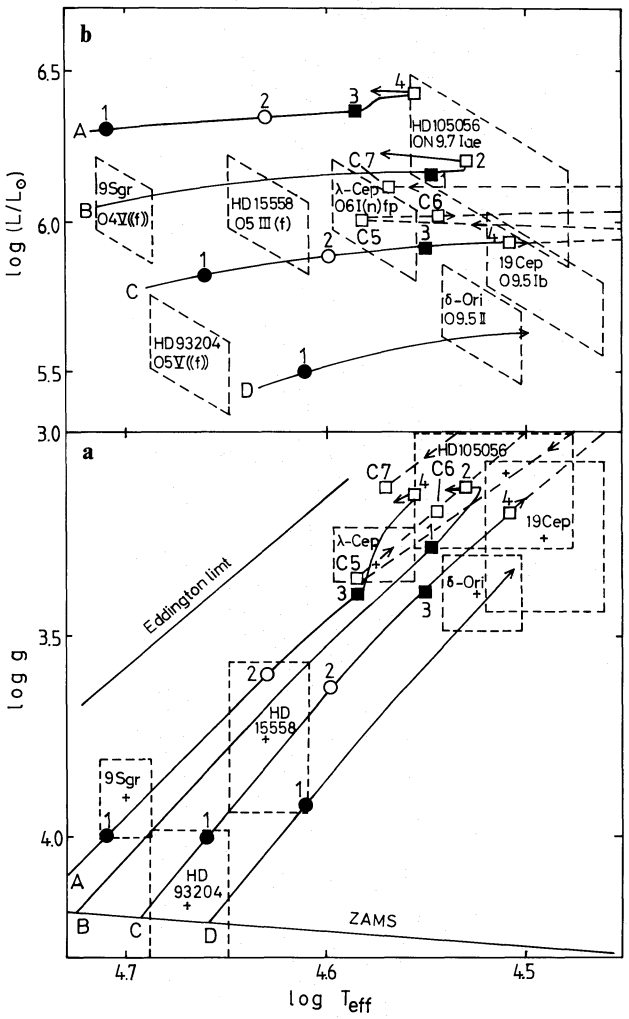

Fig. 1a and b. The ($\log g$, $\log T_{\rm eff}$) diagram (**a**) and the HR-diagram (**b**) for the wind models along evolutionary tracks of initial masses 120, 85, 60 and 40 $M_\odot$ labelled by A, B, C and D, respectively. Filled circles correspond to early O dwarfs of spectral type O3 V–O6 V, open circles to early O giants O5 III–O6 III, filled squares to bright O giants O7 II–O8 II and open squares to middle O supergiants O6 Ia/b–O9.5 Ia/b. Observed objects and error bars, representing luminosity classes V to Ia, are also shown for comparison. (For a discussion see text; the parameters of the calculated and observed objects are given in Tables 1 and 2, respectively)

$\log g$ (including the error bars shown in Fig. 1) have been adopted here. For the other objects only spectral classification and absolute visual magnitudes are available. In these cases the effective temperatures were either (HD 93204, HD 15558, λ Cep) adopted according to the He I/He II line ratios (which define the spectral type) and NLTE model atmosphere calculations reproducing these ratios (see Kudritzki et al., 1983; Simon et al., 1983; or Kudritzki and Hummer, 1986; Kudritzki et al., 1988) or (the late O supergiants of luminosity class I: 19 Cep, HD 105056) were taken to be nearly equal to the NLTE result of Voels et al. for the O 9.5 Ia supergiant α Cam (in view of this the accuracy of the effective temperatures is not better than ± 2 kK and is even worse in the case of HD 105056, since this object is obviously very close to the Eddington-limit see below). Luminosities were then obtained from the absolute magnitudes (except for HD 105056, see below) as given in the sources quoted in Table 2 (in Fig. 1 the error bars of the luminosities correspond to the accuracy of the absolute magnitudes – ± 0.3 since all objects are cluster members). The gravities were chosen in the following way: For HD 93204, which is obviously a main sequence object, a mass according to its luminosity was adopted. The same was done for the mildly evolved giant HD 15558. λ Cep as an extreme and peculiar early Of supergiant shows strong wind features in its spectrum, which indicate that it might be closer to the Eddington-limit than other objects with comparable temperature and luminosity. We have thus assumed that it is on the first loop back from the RGB and determined the mass and gravity from the MM tracks accordingly (this explains the small uncertainty of $\log g$ given in Fig. 1, but it should be noted that this gravity needs to be checked by a NLTE analysis). The gravities of 19 Cep and HD 105056 were adopted according to their luminosity classification and the NLTE result of Voels et al. for δ Ori and α Cam.

An extra comment is necessary for the luminosity of HD 105056, where the absolute magnitude is highly uncertain (see the discussion by Walborn and Panek, 1985). The value given in Table 2 was obtained using the observed terminal velocity $v_\infty = 1500\,\mathrm{km\,s^{-1}}$ (Walborn and Panek, 1985) and the relation between v_∞ and $v_{\rm esc}$ (see Abbott, 1978), where $v_{\rm esc}$ is the surface escape velocity corrected for electron scattering radiation pressure in the effective gravity. Adopting $v_\infty = (2.5 \ldots 3.0)\, v_{\rm esc}$, which is compatible with Abbott (1978) and the results of our detailed calculations (see below) this leads to

$$L = \pi\sigma T_{\rm eff}^4 v_{\rm esc}^4/(g - \sigma_{\rm E}\sigma T_{\rm eff}^4/c)^2$$

or (1)

$$\log L/L_\odot = 5.95 \text{ to } 6.27$$

($\sigma_{\rm E}$ is the electron scattering coefficient divided by density, σ is the Stefan-Boltzmann constant). In this way we obtain a luminosity and an absolute bolometric magnitude (-6.6 to -7.4), which is in rough agreement with the values quoted for other objects of the same luminosity class (see for instance Howarth and Prinja, 1988). The fact that HD 105056 is an object that shows a nitrogen anomaly has not been taken into account so far. However, it is more likely that CN burned matter shows up in the atmosphere of an evolved object of high luminosity, which once more supports the choice of the parameters in Table 2. Again, a detailed NLTE analysis is desirable for this extreme object.

The location of the seven objects of Table 2 in the HR- and ($\log g$, $\log T_{\rm eff}$)-diagram allows the models of Table 1 to be identified with different luminosity classes. Following the notation used in the compilation of UV spectra by Walborn et al. (1985) we take models A1, C1, D1 as being representative of "early O dwarfs", A2 and C2 as "early O giants", A3, B1, C3 of "bright O giants" and A4, B2, C4, 5, 6, 7 as "middle O supergiants". In the following we shall compare the computed spectral morphology with the observations of each class. Moreover, we shall discuss the calculated dynamical properties of their winds.

3. Results

Table 3 summarizes the results of the computations with respect to the wind dynamics and gives $\dot{M}$ and v_∞ together with the mean force multiplier parameters k, α, δ. They will be discussed in detail in 3.3. However, we first discuss them in the context of the spectral morphology.

Table 1. Parameters of O stars along evolutionary tracks. Tracks of initial masses 120, 85, 60 and 40 $M_\odot$ are labelled by A, B, C and D, respectively. The Arabic numerals represent different luminosity classes (see Fig. 1)

	A (M_{ZAMS} = 120 $M_\odot$)				B (M_{ZAMS} = 85 $M_\odot$)		C (M_{ZAMS} = 60 $M_\odot$)							D (M_{ZAMS} = 40 $M_\odot$)
	1	2	3	4	1	2	1	2	3	4	5	6	7	1
T_{eff} (kK)	51.28	42.66	38.46	35.81	35.16	34.08	45.71	39.63	35.48	32.17	38.28	35.00	37.00	40.83
$R/R_\odot$	18.0	27.4	34.0	42.0	32.1	36.0	12.9	18.5	23.9	29.8	22.7	27.6	27.6	11.2
$\log(L/L_\odot)$	6.30	6.34	6.36	6.42	6.15	6.20	5.82	5.88	5.91	5.93	6.00	6.02	6.11	5.49
log(g)	4.0	3.6	3.4	3.15	3.284	3.135	4.0	3.634	3.4	3.2	3.36	3.19	3.13	3.92
v_{esc} (km/s)	1179.	839.	722.	454.	648.	498.	1092.	836.	703.	609.	535.	470.	317.	1008.
luminosity class	V	III	II	I	II	I	V	III	II	I	I	I	I	V

Table 2. Parameters for observed O stars. Note that the luminosity given by de Jager et al. (1988) for δ Ori has been corrected for the higher T_{eff} obtained by Voels et al. (1988)

star	spectral type	$\log(T_{eff})$	log(g)	$\log(L/L_\odot)$
9 Sgr	O4 V ((f))	4.70 (1)	3.9 (1)	6.03 (2)
HD 93204	O5 V ((f))	4.67 (3,4)	4.2 (4,3)	5.56 (3)
HD 15558	O5 III (f)	4.63 (4)	3.8 (4)	6.0 (4)
δ Ori	O9.5 II	4.52 (1)	3.4 (1)	5.64 (2)
λ Cep	O6 I(n) fp	4.57 (5)	3.3 (*)	6.00 (5)
19 Cep	O9.5 Ib	4.50 (*,1,5)	3.25 (*,1,5)	5.75 (5)
HD 105056	ON9.7 Iae	4.50 (*,1)	3.1 (1,6)	6.04 (*)

(1) Voels et al. (1988)
(2) de Jager et al. (1988)
(3) Garmany et al. (1981)
(4) Howarth and Prinja (1988)
(5) Abbott (1978)
(6) Walborn and Panek (1985)
(*) This paper

Table 3. Terminal velocities, mass-loss rates and parameters of the force multiplier for the wind models

	A (M_{ZAMS} = 120 $M_\odot$)				B (M_{ZAMS} = 85 $M_\odot$)		C (M_{ZAMS} = 60 $M_\odot$)							D (M_{ZAMS} = 40 $M_\odot$)
	1	2	3	4	1	2	1	2	3	4	5	6	7	1
v_∞ (km/s)	4490.	2930.	2700.	1300.	2700.	1850.	4560.	2825.	2650.	3125.	2120.	1420.	790.	3650.
$\dot{M}$ ($10^{-6} M_\odot$/yr)	6.5	8.4	7.6	16.0	4.05	6.3	1.43	1.78	1.63	1.08	4.20	4.10	50.7	0.51
Γ	.444	.528	.569	.762	.514	.647	.286	.364	.408	.436	.611	.640	.850	.214
$\bar{\rho}_w$ (10^{-12} ($M_\odot$/yr)/($R_\odot^2$ km/s))	4.468	3.817	2.435	6.977	1.459	2.623	1.884	1.841	1.077	0.389	3.845	3.790	84.24	1.114
k	.055	.055	.056	.049	.044	.054	.052	.058	.043	.024	.064	.057	.147	.060
α	.707	.696	.682	.690	.708	.685	.712	.678	.696	.737	.680	.662	.664	.681
δ	.086	.089	.061	.074	.028	.029	.067	.075	.064	.037	.018	.062	.032	.067

3.1. *The morphology of stellar wind spectra*

3.1.1. Si IV

A characteristic feature of O star mass-loss is the strong dependence of the Si IV resonance doublet on luminosity class. Figure 2 demonstrates that this is in principle reproduced by the theory. For early O dwarfs only weak photospheric lines are produced, in agreement with the observations, where it is not clear whether lines are interstellar or photospheric and whether additional blends contribute (Fig. 2a). The same is true for the giants, where very minor indications of winds are present in both theory and observations (Fig. 2b). For the bright giants (Fig. 2c) wind effects are definitely present in the calculations, manifested in blue shifted absorption rather than in redward emission.

Qualitatively, this agrees with the observation. (Note that the "noise" in the theoretical profile is the result of an inadequate depth discretization in our calculations. While this is of no importance for the objectives of the work presented here, it will be improved in future work). For the supergiants typical P-Cygni structures are obtained matching the observations in surprising detail (Fig. 2d). Note that the differences in the profiles between models C4, B2, C5 and A4, C6 are caused by the differences of v_∞, so that e.g. the emission peak seen clearly in C6 is filled by the absorption trough of the second component in C4. A thorough discussion of the physical background of the luminosity dependence of Si IV will be given in the next subsection.

3.1.2. C IV N V

In contrast to Si IV, the resonance doublets of C IV and N V have a P-Cygni structure independent of luminosity class. This is also reproduced by the theory as demonstrated by Figs. 3 and 4. The qualitative agreement is again acceptable. However, several details will need further investigation. For the O dwarfs the v_∞ of

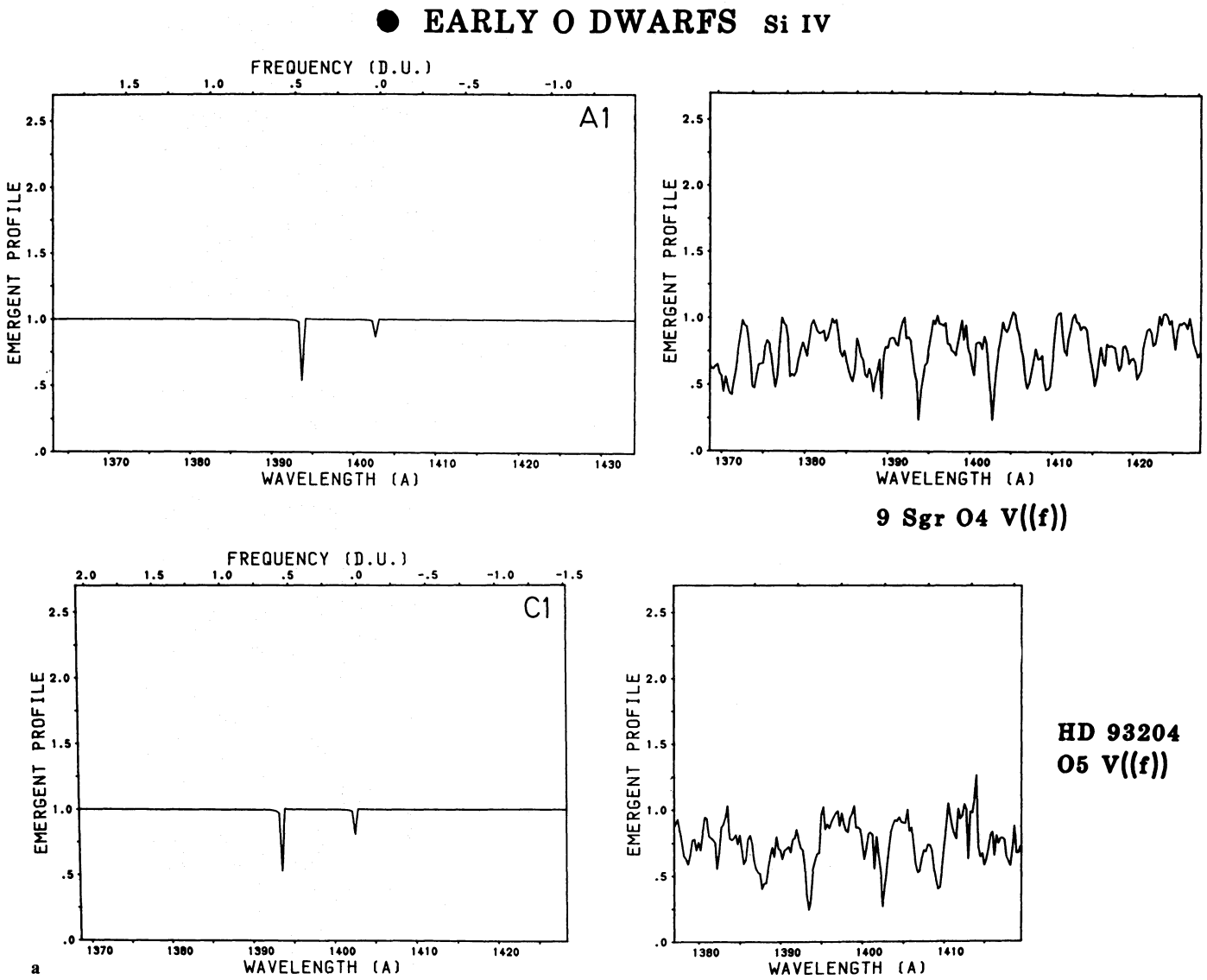

Fig. 2a–d. Si IV ($\lambda\lambda$ 1394, 1403) profiles across the O star domain; the wind model lines are compared with corresponding observed IUE P-Cygni profiles (observations are taken from Walborn et al., 1985) displaying the strong observed luminosity effect of Si IV as reproduced by the calculated wind models (the observed objects are labelled with HD numbers (names) and spectral types, and the wind models are labelled with the symbols shown in Fig. 1)

O EARLY O GIANTS

Si IV

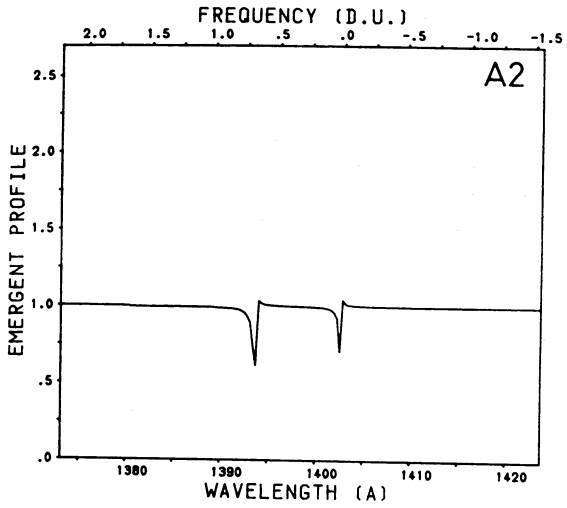

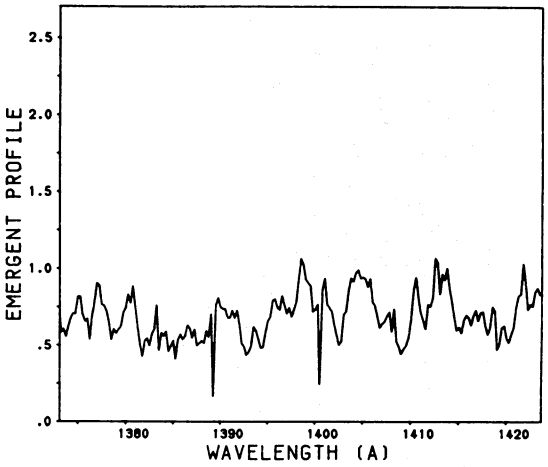

HD 15558

O5 III(f)

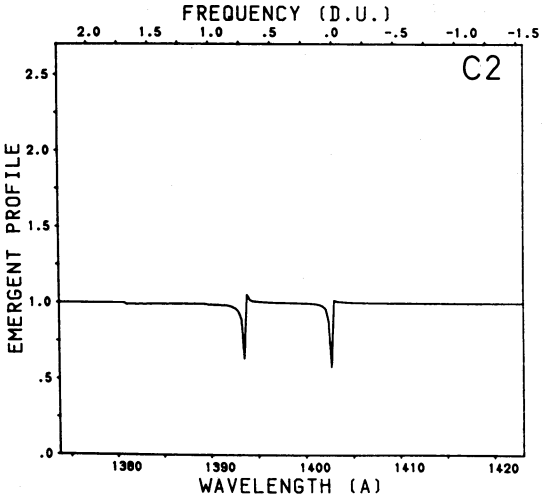

Fig. 2b

■ BRIGHT GIANTS

Si IV

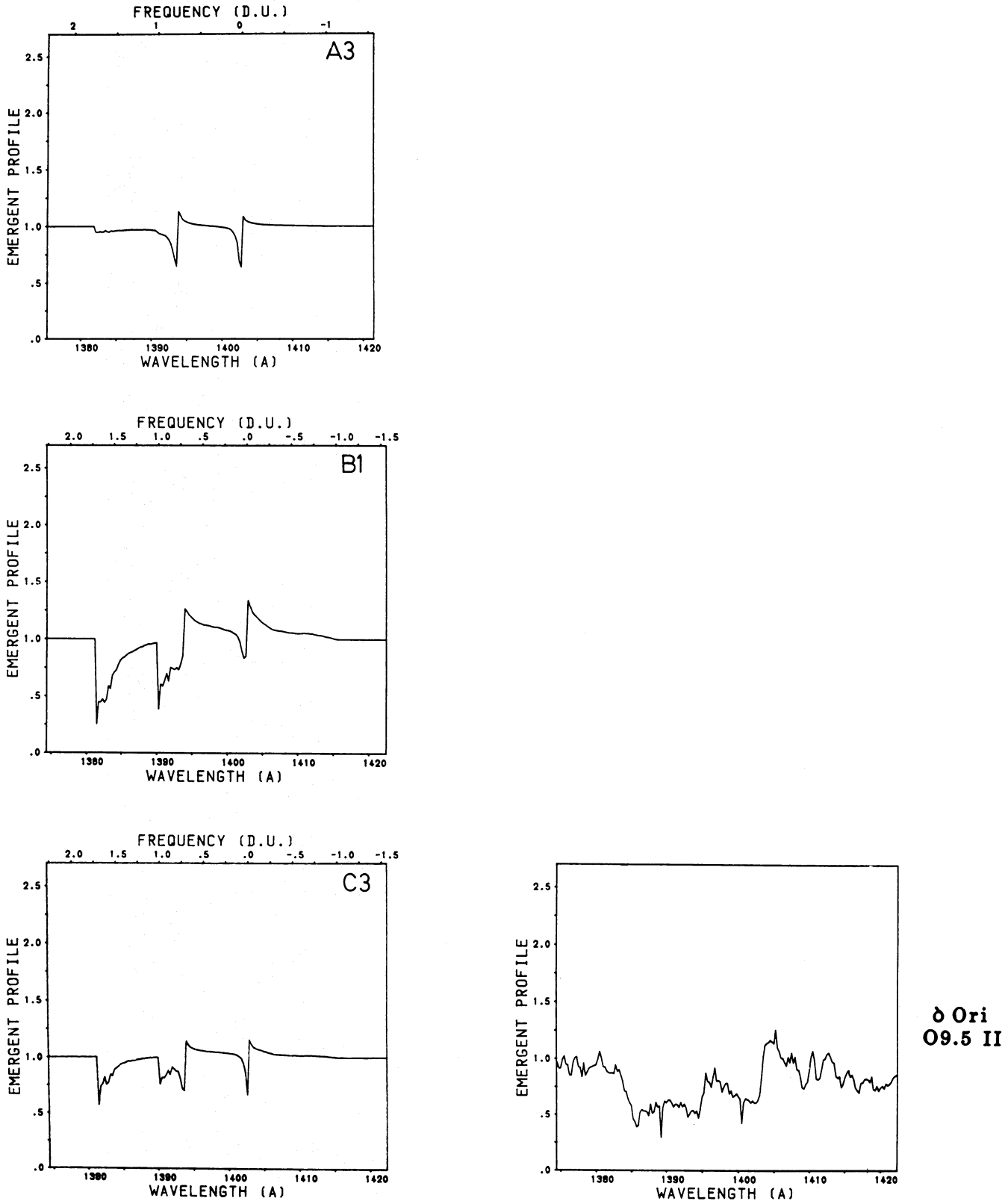

Fig. 2c

□ MIDDLE Of SUPERGIANTS

Si IV

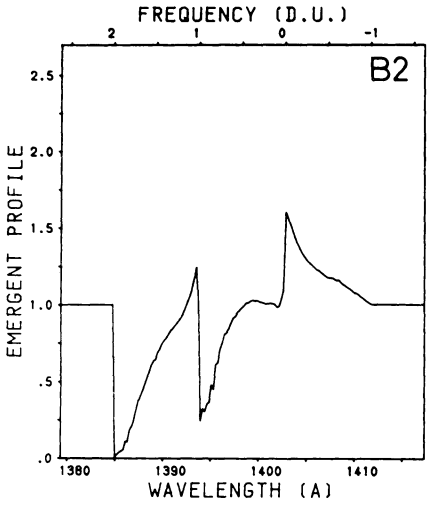

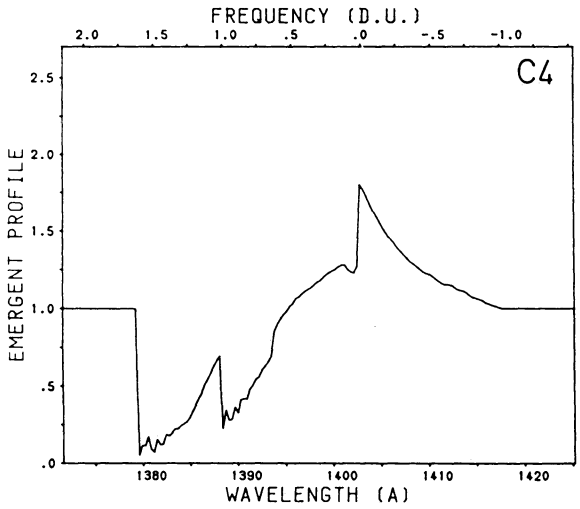

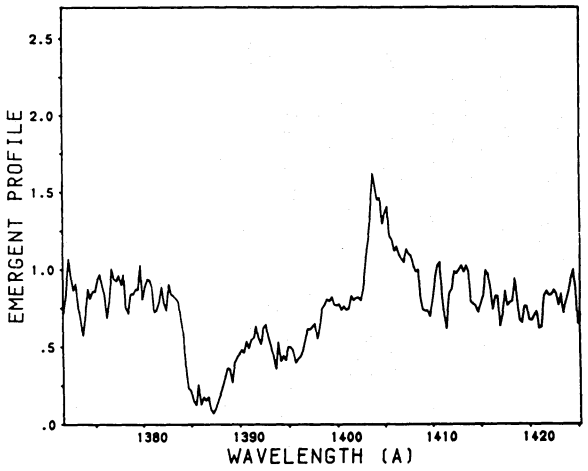

19 Cep
O9.5 Ib

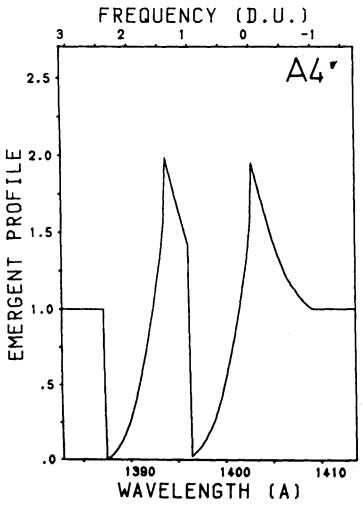

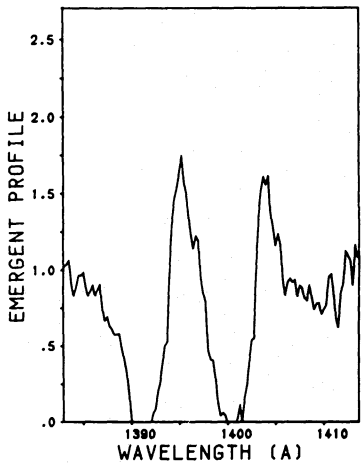

HD 105056
ON9.7 Iae

Fig. 2d

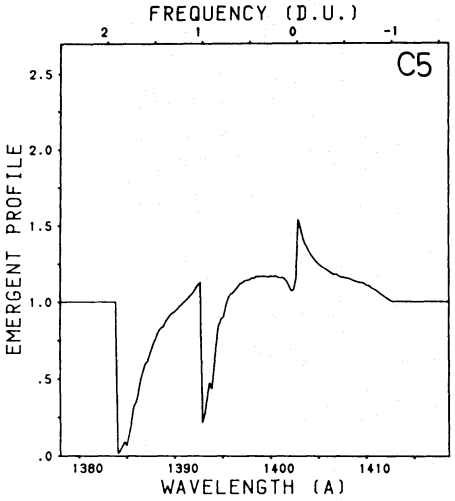

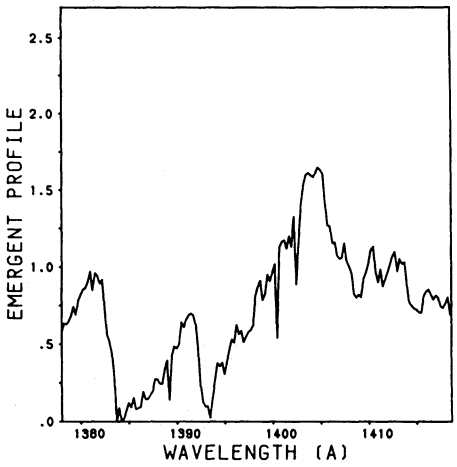

λ Cep
O6 I(n)fp

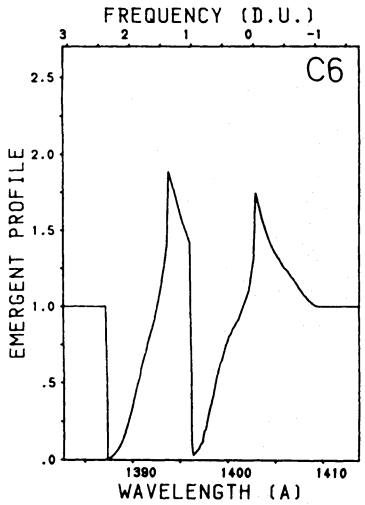

Fig. 2d (continued)

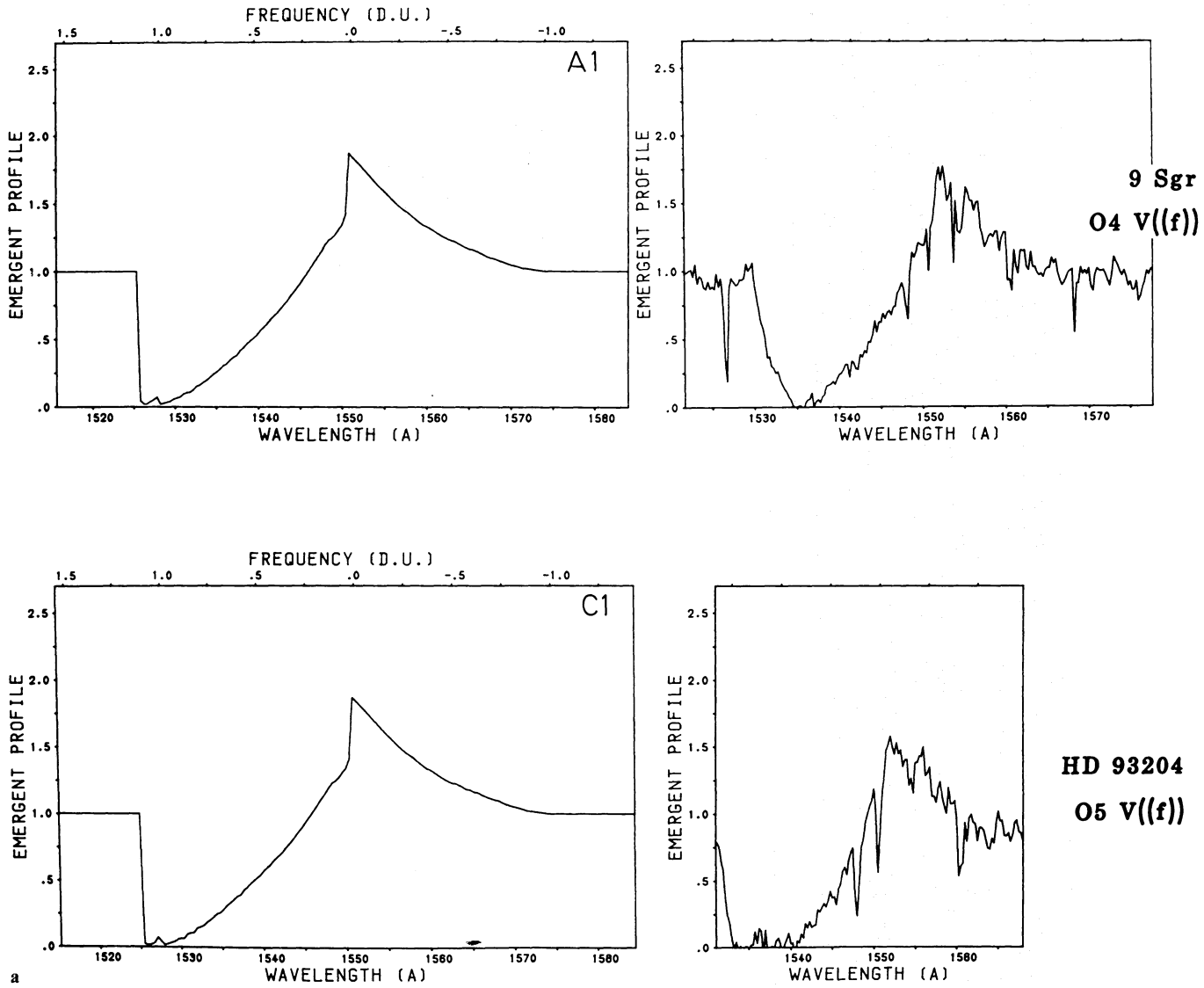

a

Fig. 3a–d. Same as Fig. 2, but for C IV ($\lambda\lambda$ 1548, 1551) profiles

O EARLY O GIANTS

C IV

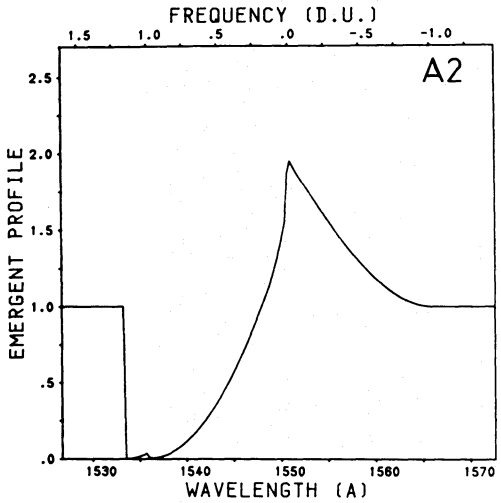

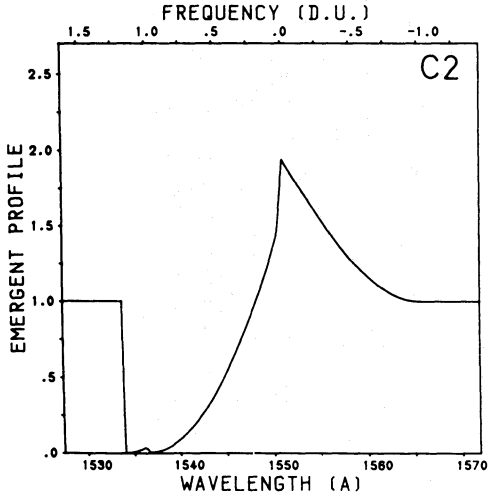

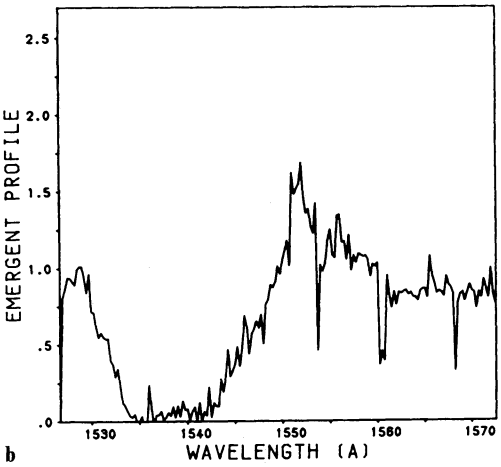

b

HD 15558

O5 III(f)

Fig. 3b

■ BRIGHT GIANTS

C IV

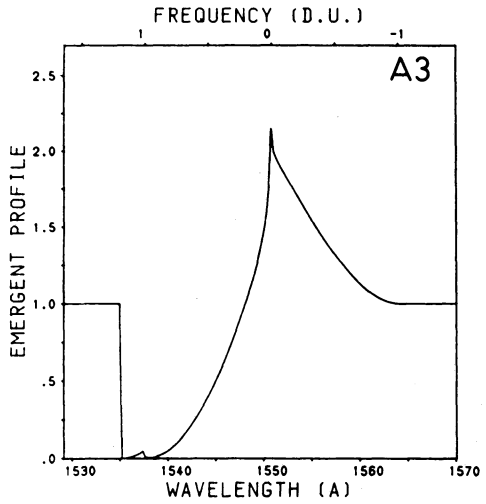

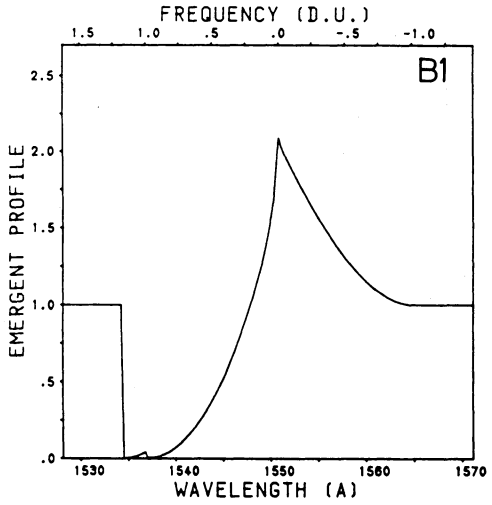

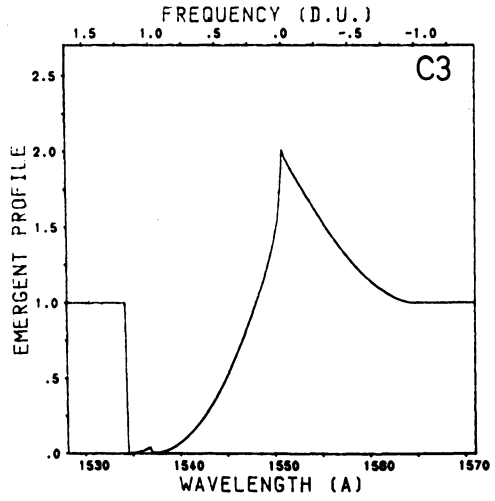

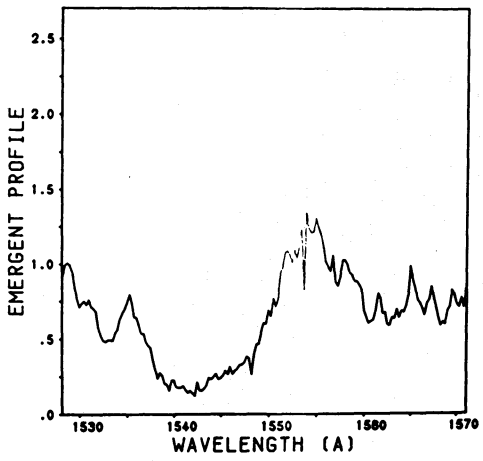

δ Ori

O9.5 II

Fig. 3c

□ MIDDLE Of SUPERGIANTS

C IV

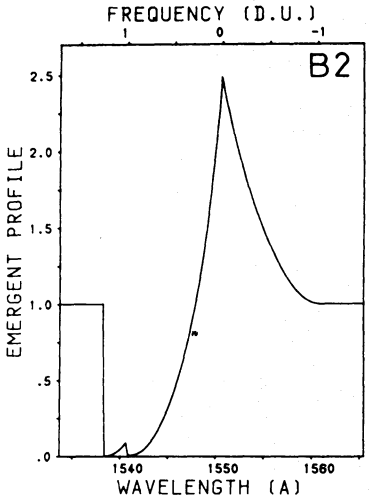

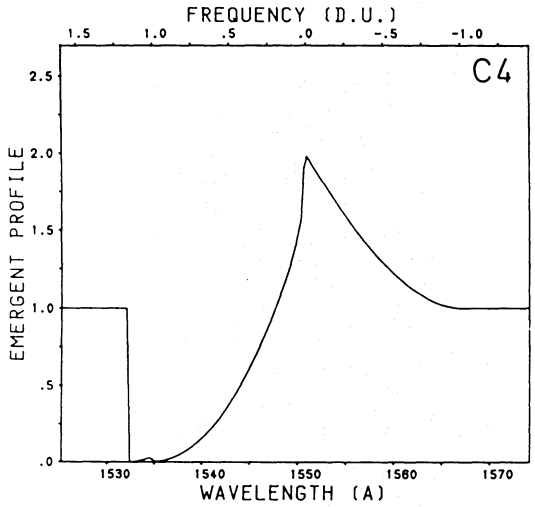

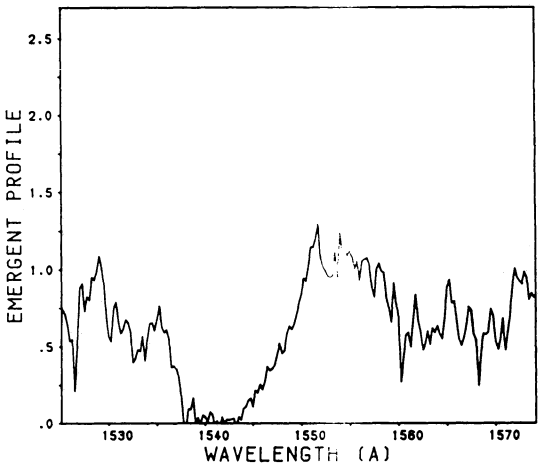

19 Cep
O9.5 Ib

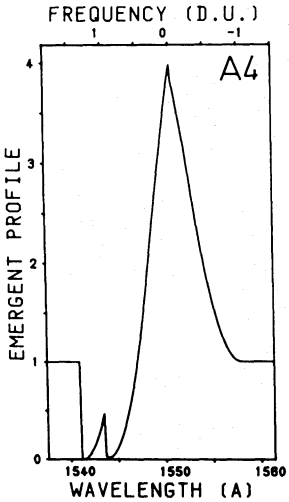

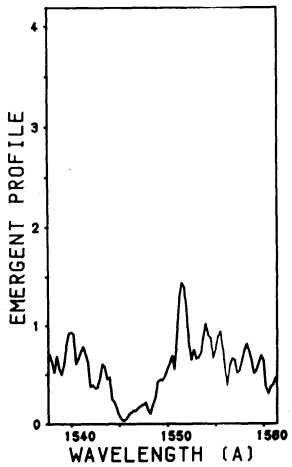

HD 105056
ON9.7 Iae

Fig. 3d

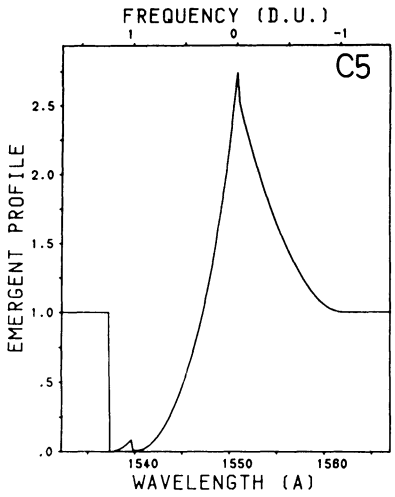

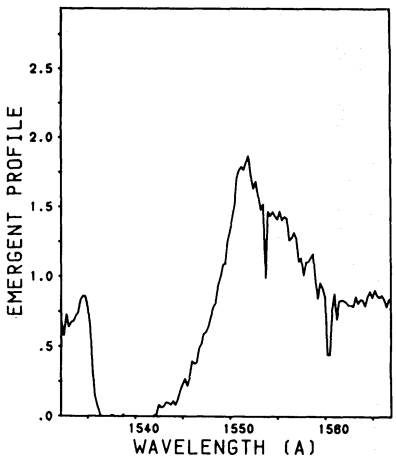

λ Cep
O6 I(n)fp

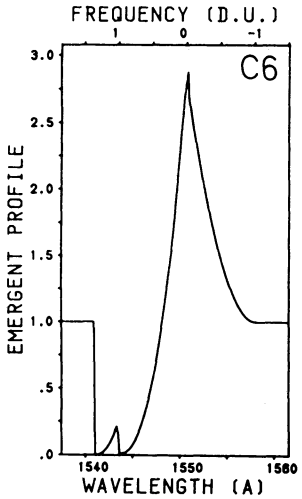

Fig. 3d (continued)

● EARLY O DWARFS

N V

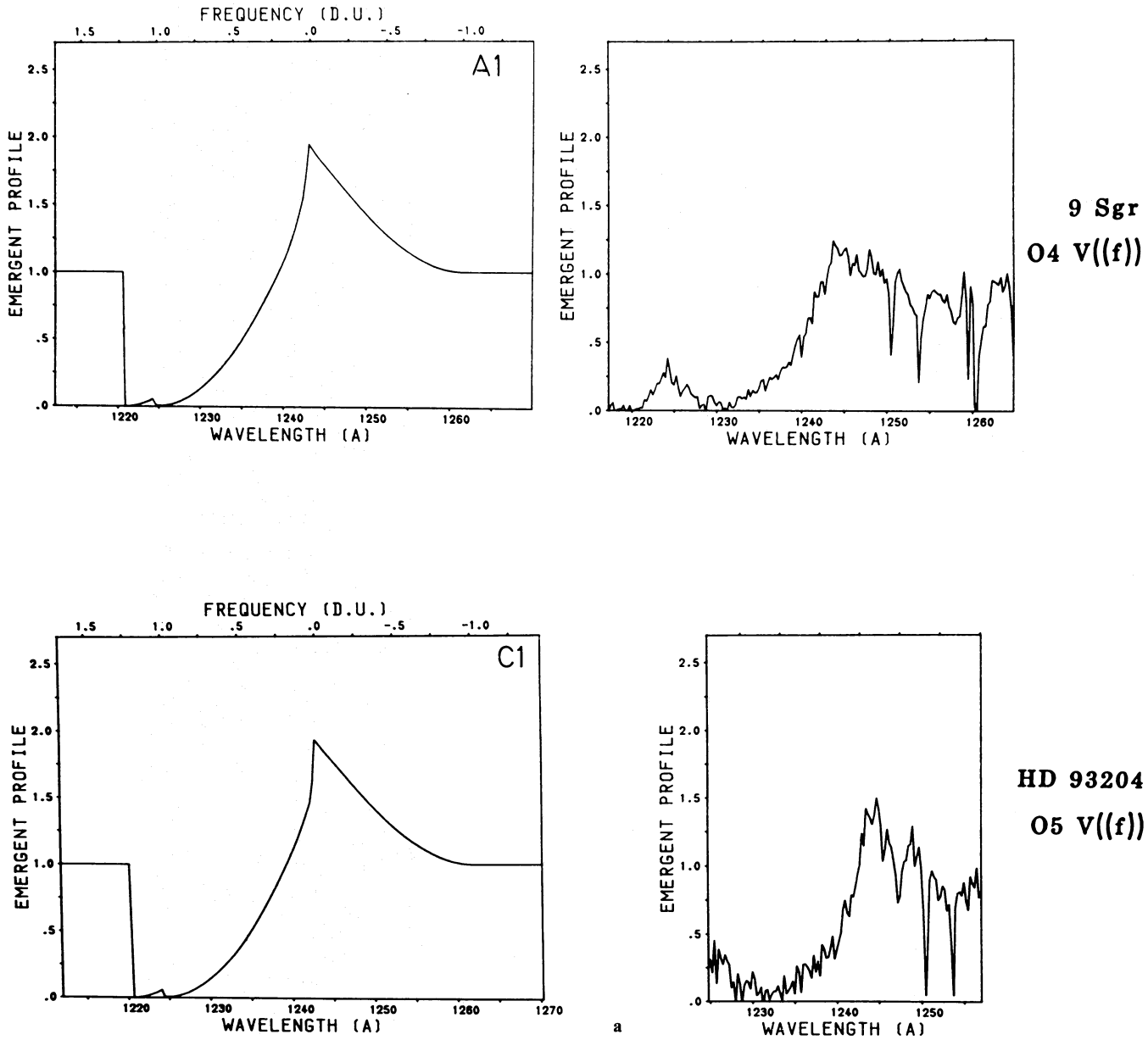

Fig. 4a–c. Same as Fig. 2, but for N v ($\lambda\lambda$ 1239, 1243) profiles. (Note that the early O giants are not compared, since the absorption part of the observed N v profiles are too strongly influenced by interstellar Ly α absorption)

■ BRIGHT GIANTS

N V

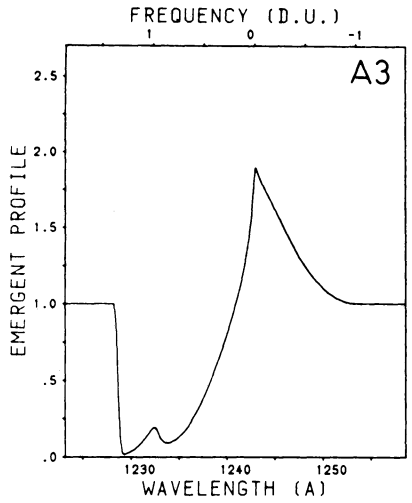

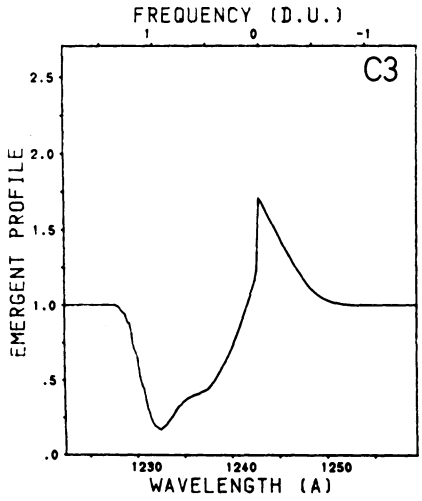

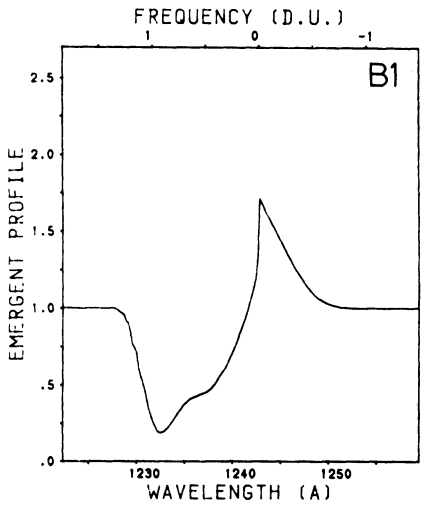

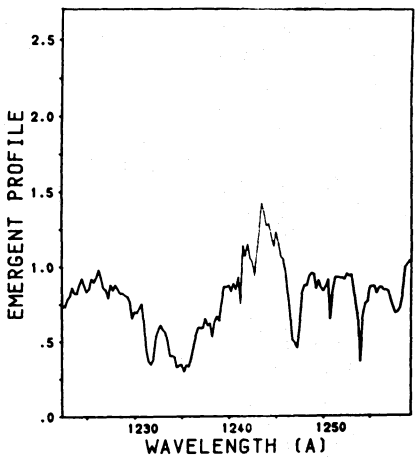

δ Ori

O9.5 II

Fig. 4b

□ MIDDLE Of SUPERGIANTS

N V

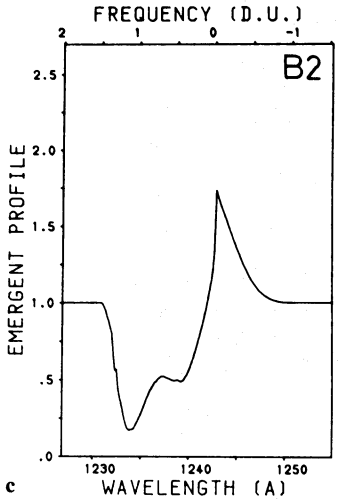

c

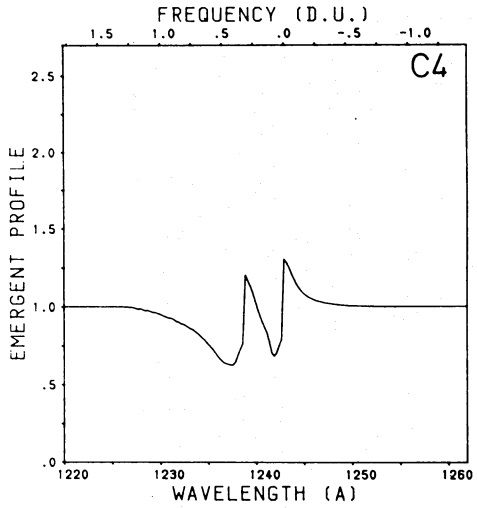

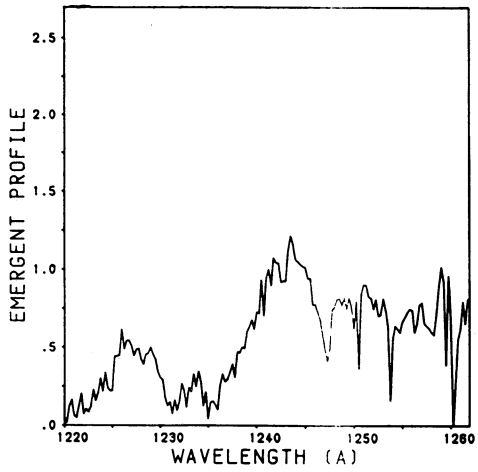

19 Cep

O9.5 Ib

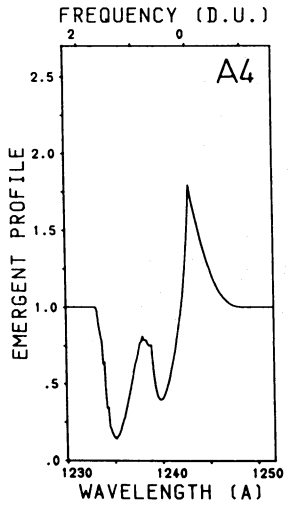

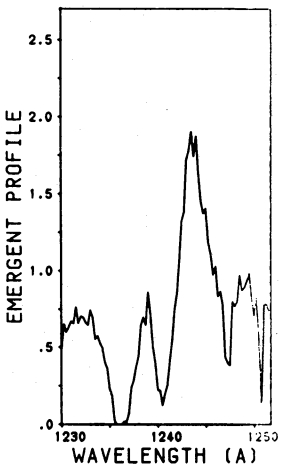

HD 105056

ON9.7 Iae

Fig. 4c

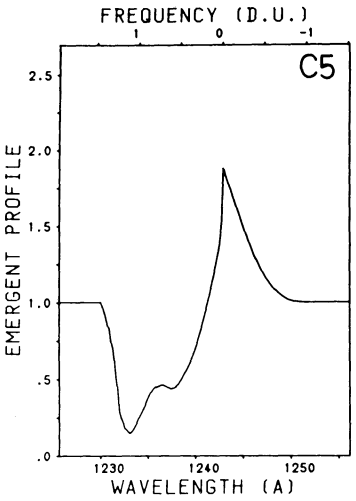

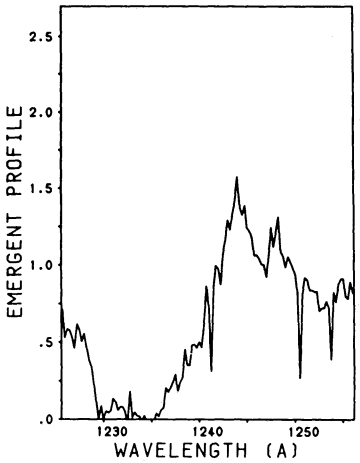

λ Cep
O6 I(n)fp

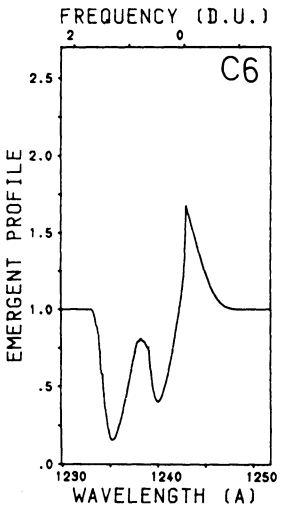

Fig. 4c (continued)

the models are too large and the detailed shape of the profiles is not matched exactly. However, we are optimistic that this can be improved by the use of different models within the uncertainties of the stellar parameters. The observed C IV profile of δ Ori is unsaturated with weak emission whereas all theoretical profiles are stronger. A NLTE determination of the carbon abundance from photospheric lines will show whether this is an abundance effect. In the case of the supergiants the same effect is encountered for λ Cep, 19 Cep and very strongly for HD 105056. Since the latter object is an ON star, it is very likely that the carbon abundance is strongly reduced due to mixing of CN-cycled material into the atmosphere and that nitrogen is enhanced (Schönberner et al., 1988). The inspection of the N V profiles confirms this. A similar effect might account for 19 Cep and λ Cep, since the recent analysis of apparently normal late O and B supergiants (Voels et al., 1988; Kudritzki et al., 1988) has revealed that these objects also have mildly enhanced helium abundances indicating the presence of CN-cycle processed material in the photospheres of these stars.

3.1.3. N IV

The NLTE multi-level treatment of our radiation driven wind code also allows us to calculate the subordinate line N IV λ 1718, another typical wind line. Figure 5 shows that the situation of the theory is still far from being perfect but by no means hopeless. We will have to wait until the necessary improvement in the atomic models and data for N V/IV/III (see Sect. 2 and Pauldrach, 1987) and the inclusion of multi-line effects (see Puls, 1987) have been made. This is part of our future work.

3.1.4. O VI

An important observation obtained several years ago with the Copernicus satellite concerns the presence of the O VI ($\lambda\lambda$ 1031.9, 1037.6) resonance doublet in the wind spectra of O stars. Pauldrach (1987) showed for the case of the O4 f star ζ Puppis that the detailed multi-level NLTE treatment yields observable O VI for cool wind models with $T_{\rm wind} \approx T_{\rm eff}$ without any further source of ionisation. Our calculations now allow the parameter

N IV

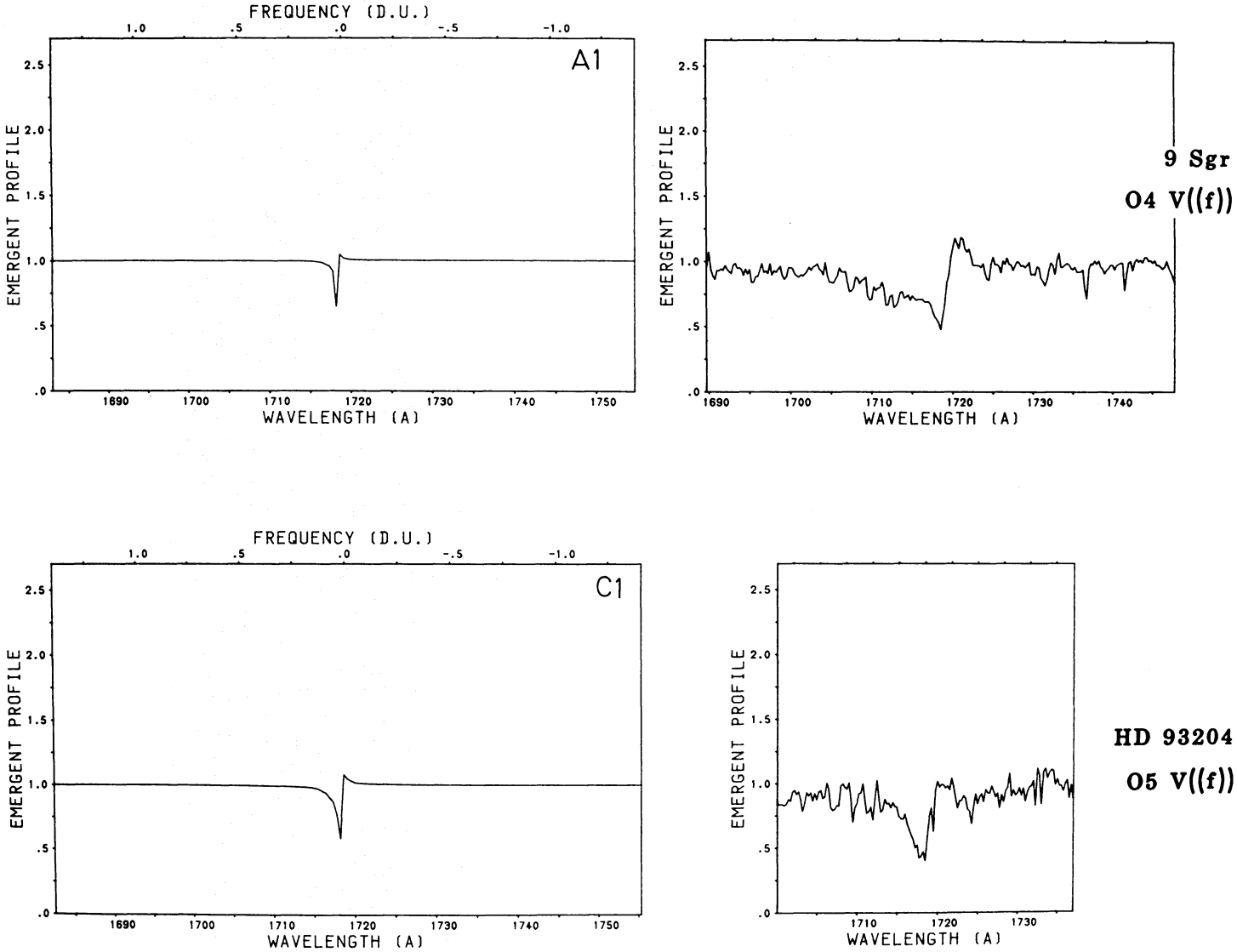

Fig. 5a–d. Same as Fig. 2, but for a subordinate line of N IV (λ 1718)

O EARLY O GIANTS

N IV

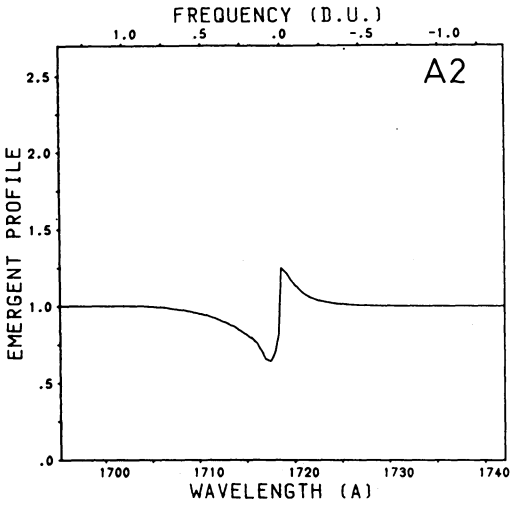

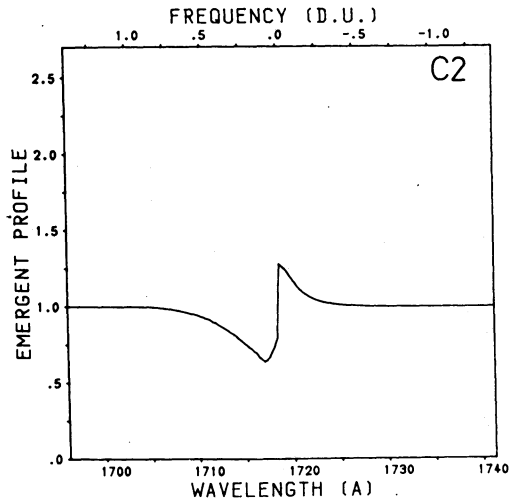

Fig. 5b

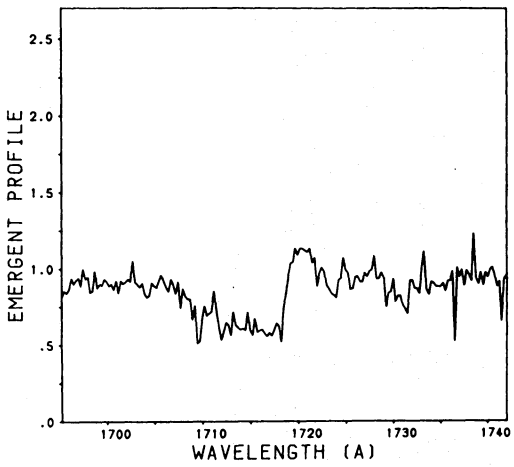

HD 15558

O5 III(f)

■ BRIGHT GIANTS

N IV

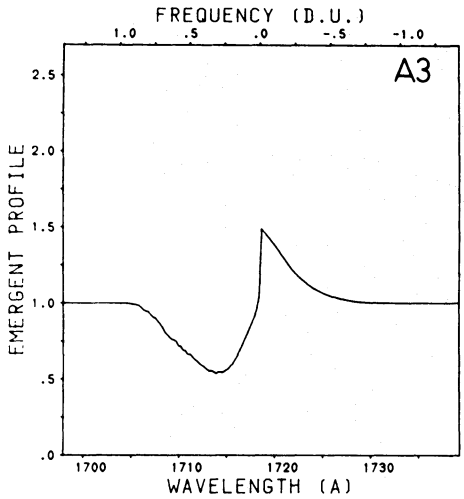

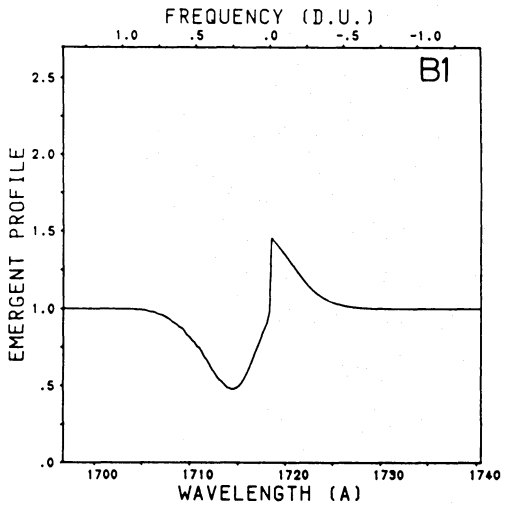

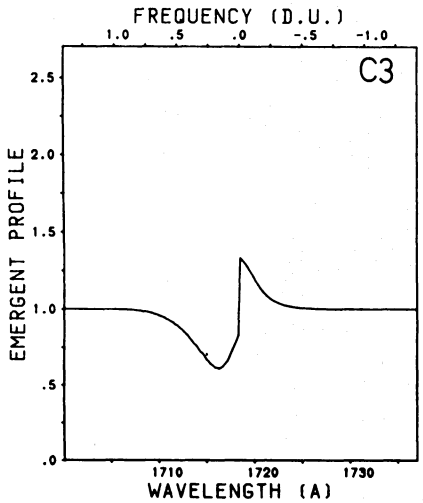

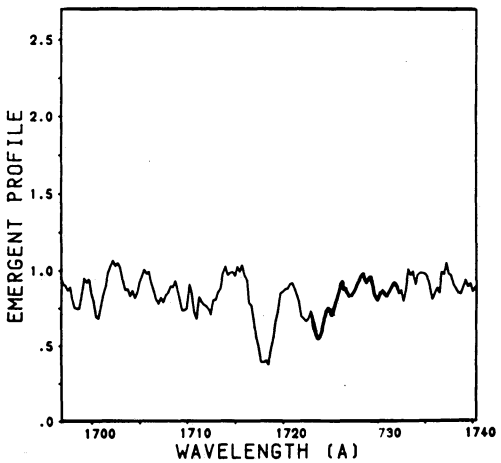

δ Ori

O9.5 II

Fig. 5c

□ MIDDLE Of SUPERGIANTS

N IV

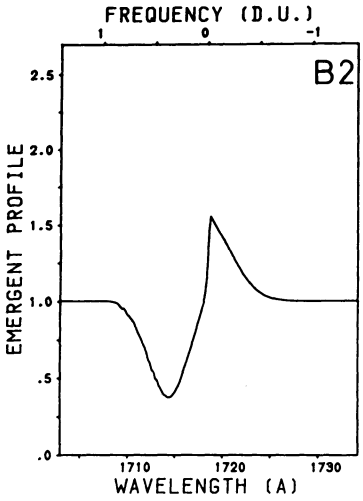

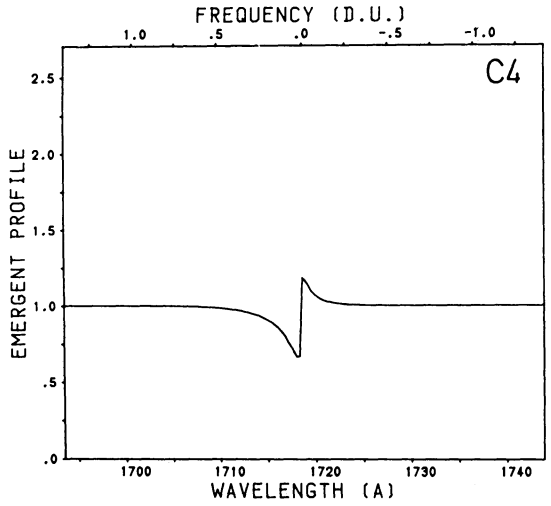

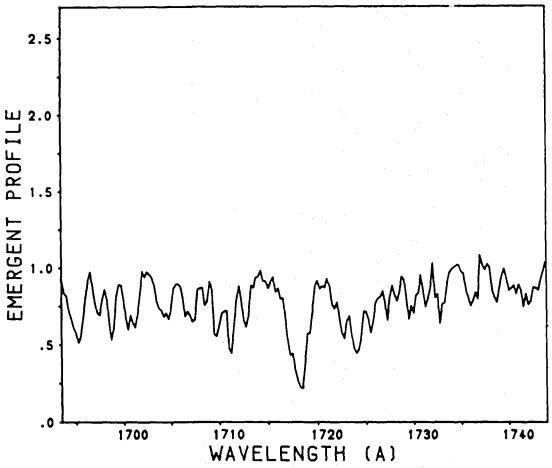

19 Cep
O9.5 Ib

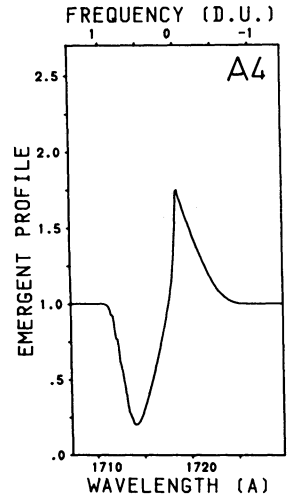

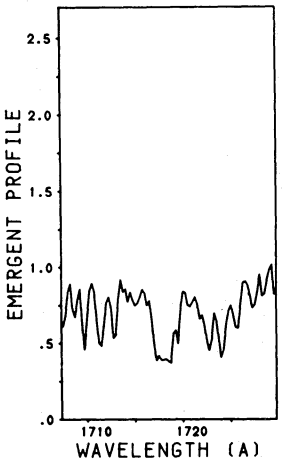

HD 105056
ON9.7 Iae

Fig. 5d

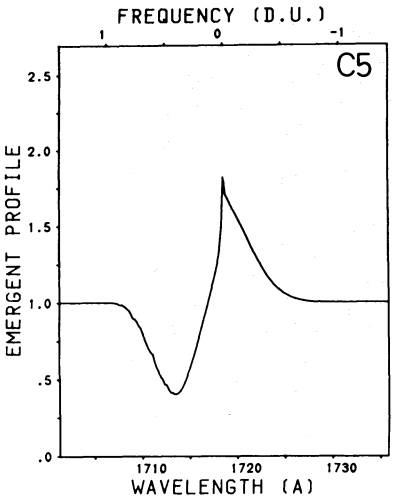

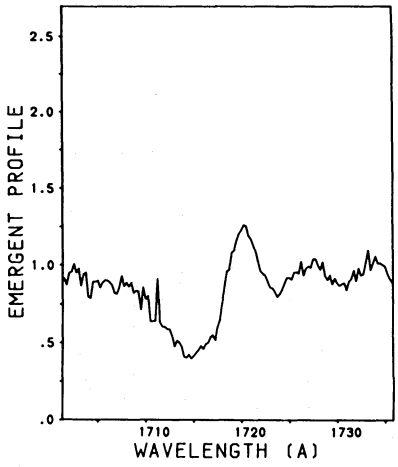

λ Cep
O6 I(n)fp

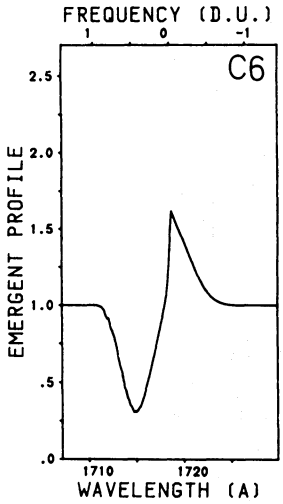

Fig. 5d (continued)

domain where the NLTE wind calculations are able to produce observable O VI to be delimited. Figure 6a illustrates the situation: The two hotter dwarf models (A1, C1) give well developed O VI P-Cygni profiles whereas the cool model (D1) shows only a week O VI line. Since we encountered weak O VI lines also for model C2 in the case of early O giants and for model A3 in the case of bright giants, the models predict obviously a dramatic dependence of O VI on effective temperature in our sample of O stars. This gives rise to a border line at $T_{\rm eff} \approx 38\,{\rm kK}$ (corresponding to spectral type O6), which restricts the occurrence of O VI profiles. Besides the *pronounced dependence on temperature* the theoretical O VI balance is also luminosity dependent, since models A3 and C2 show a stronger wind component than the somewhat hotter model D1 on the main sequence. Since this is an unexpected behaviour we will discuss the physical reason for this in the next subsection. None of the supergiant models (A4, B2, C5, 6, 7) develop an observable O VI line, *since the ionising radiation fields are too weak in this temperature range*, because the continua shortward of the He II edge are optically thick. This leads to a more precise definition of the theoretical boundaries for O VI in the HR-diagram, which when compared with the observations given by Snow and Jenkins (1977) and Olson and Castor (1981), *reveal an obvious discrepancy*. This can be interpreted as follows. For the hotter O stars the intense atmospheric EUV radiation field dominates the ionisation and excitation processes and thus the multi-level NLTE treatment by Pauldrach (1987) is probably sufficient to describe the situation. For the cooler O stars, however, the EUV radiation field is weaker and therefore the diffuse X-ray radiation field, which has been detected as an ubiquitous feature of all O stars, may dominate the ionisation. Consequently, our treatment, in which the X-rays are ignored, becomes inadequate. We repeat here the statement of Pauldrach (1987) that it is possible to include Auger-ionization in our code provided the local X-ray radiation field in the wind

● EARLY O DWARFS

A1

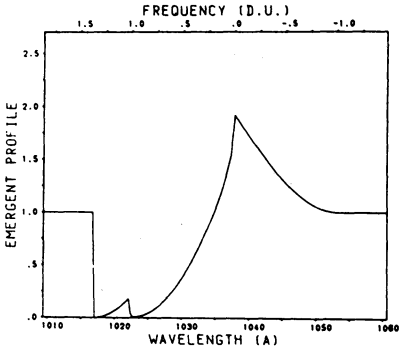

C1

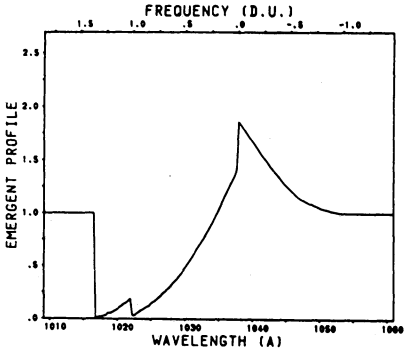

D1

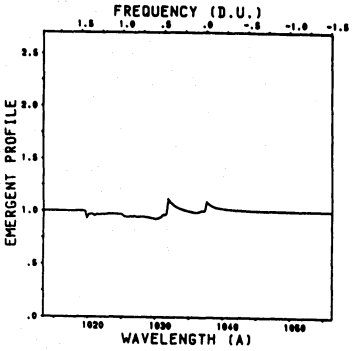

o EARLY O GIANTS

A2

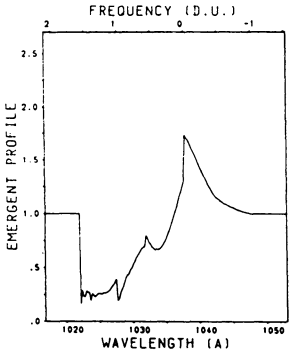

C2

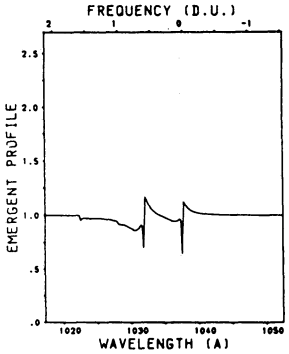

■ BRIGHT GIANTS

A3

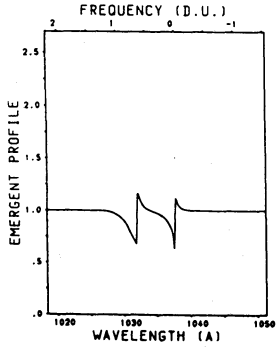

Fig. 6a. O VI P-Cygni profiles of the wind models as a function of spectral type (horizontal) and luminosity class (vertical) (for a discussion see text)

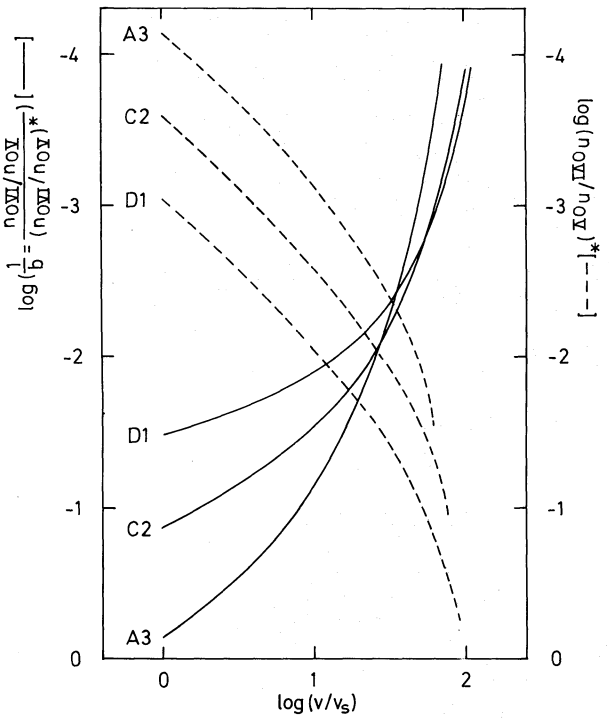

Fig. 6b. The O VI departure coefficient (fully drawn) and the corresponding Saha-Boltzmann factor (dashed) versus the velocity for the models A3, C2 and D1. This diagram shows the origin of the luminosity dependence of the O VI resonance line (for a discussion see text)

is given. This will be included together with additional refinements, that might influence the theoretical O VI borderline, in the forthcoming work.

3.2.1. An explanation of the Si IV luminosity effect

The resonance lines of Si IV and C IV (or N V) behave significantly differently. C IV remains a typical saturated P-Cygni line independent of stellar parameters, whereas Si IV shows a strong luminosity dependence. The reason for the constant behaviour of C IV is simple. Over the range of O star parameters the ground state of this ion is so strongly populated that changes in the population are hidden by the saturation effects. Thus, this line is ideal for the measurement of v_∞ (unless the effects of the CN-burning have drastically reduced the carbon abundance). However, because of its strong saturation it is almost useless for the determination of $\dot{M}$. The situation is completely different for silicon. Here the dominant ionisation stage is Si V (see Table 5), which has a noble gas atomic structure and an extremely high ionisation energy. Si IV with its smaller ionization energy of 45.14 eV, corresponding to $\lambda_{ion} = 274.66$ Å is only a trace ion and this leads to a resonance line of moderate optical thickness. Since Si IV is ionized by photons longward of the He II edge (228 Å), the corresponding ionising continuum is optically thin in almost all cases (except winds of very high density extremely close to the Eddington-limit as exemplified by model C7) and thus the assumption of a geometrically diluted radiation field is correct to first order. Consequently, the approximate treatment of the ionization equilibrium between Si IV and V in terms of modified recombination theory (Abbott, 1982; Abbott and Lucy, 1985; Pauldrach, 1987, Eq. (12) is not too bad an estimate.

$$X^*(\mathrm{Si\,IV}) = \frac{n_1(\mathrm{Si\,IV})}{N_{\mathrm{total}}(\mathrm{Si})} \approx \left(\frac{T_R}{T_E}\right)^{1/2} \frac{n_E}{W} \left(\frac{n_{1,\mathrm{Si\,IV}}}{n_{1,\mathrm{Si\,V}} n_e}\right)^*_{T_R} \qquad (2)$$

X is the ionization fraction of Si IV, T_R the photospheric radiation temperature at the frequency of the continuum ground level transition, W the dilution factor, T_E the electron temperature in the wind and $(\ )^*_{T_R}$ denotes the Saha-Boltzmann factor using T_R. To simplify the discussion further we set $T_R = T_{\mathrm{eff}}$ and concentrate on those wind layers where $v(r)$ has almost reached v_∞. Here we have $n_E/W = const. \times \dot{M}/(v_\infty R^2)$ so that we can obtain a simplification of X^* in the following form

$$\log X^*(\mathrm{Si\,IV}) = -1.845 + \frac{266}{T_{\mathrm{eff}}}[\mathrm{kK}] - \frac{3}{2}\log T_{\mathrm{eff}}[\mathrm{kK}] + \log \bar{\rho}_w$$

$$\log \bar{\rho}_w = -\log v_\infty [\mathrm{km\,s^{-1}}] - 2\log\frac{R}{R_\odot} + \log \dot{M}[10^{-6} M_\odot\,\mathrm{yr}^{-1}] \qquad (3)$$

$\bar{\rho}_w = \dot{M}/(v_\infty R_*^2)$ corresponds to the mean density of the stellar wind. (The constant -1.845 represents the normalization to model D1).

Figure 7a demonstrates that the approximation Eq. (3) is a reasonable first estimate. For the cooler models (A4, B1, B2, C3, C5, C4, C6 and C7), the differences are caused by strong photospheric line blocking of the Kurucz models that yield $T_R < T_{\mathrm{eff}}$ (see Table 4). This enhances X(Si IV) in the correct treatment, because less ionising flux is available than adopted in Eq. (3). The same is true for model C7, which is optically thick in the Si IV continuum due to the enormous density of its wind and where the ionizing radiation field is given by local emission and absorption of the wind plasma in the correct numerical treatment. Despite these difficulties, formula (3) allows the basic dependence of Si IV on the stellar parameters to be understood.

Table 4. Comparison of effective temperatures and radiation temperatures at the frequency of the Si IV ionisation edge

	A ($M_{ZAMS} = 120\ M_\odot$)				B ($M_{ZAMS} = 85\ M_\odot$)		C ($M_{ZAMS} = 60\ M_\odot$)							D ($M_{ZAMS} = 40\ M_\odot$)
	1	2	3	4	1	2	1	2	3	4	5	6	7	1
$\log(T_{\mathrm{eff}})$	4.710	4.630	4.585	4.554	4.546	4.533	4.660	4.598	4.550	4.507	4.583	4.544	4.568	4.611
$\log(T_{R_{\mathrm{SiIV}}})$	4.781	4.697	4.598	4.465 =====	4.462 =====	4.460 =====	4.708	4.602	4.464 =====	4.319 =====	4.471 =====	4.463 =====	opt.thick	4.606

Table 5. Ionisation ratios of some typical elements (dashes indicate values n_{ion}/n_H lower than 10^{-9})

	A (M_{ZAMS} = 120 $M_\odot$)				B (M_{ZAMS} = 85 $M_\odot$)		C (M_{ZAMS} = 60 $M_\odot$)							D (M_{ZAMS} = 40 $M_\odot$)
	1	2	3	4	1	2	1	2	3	4	5	6	7	1
n_H (cm^{-3})	2.1(10)	1.8(10)	1.2(10)	3.2(10)	6.6 (9)	1.2(10)	9.1 (9)	8.7 (9)	5.1 (9)	1.9 (9)	1.9(10)	1.9(10)	1.8(11)	5.3 (9)
n_E/n_H	1.21	1.21	1.21	1.15	1.20	1.17	1.21	1.20	1.20	1.16	1.19	1.15	1.16	1.21
n_{Ion}/n_H														
CIII	-	-	-	1.4(-7)	3.8(-8)	7.9(-8)	-	-	1.4(-8)	6.8(-6)	4.1(-8)	9.1(-8)	6.4(-6)	-
CIV	1.7(-7)	1.4(-6)	1.6(-5)	3.7(-4)	3.0(-4)	3.8(-4)	5.2(-7)	5.8(-6)	1.9(-4)	4.6(-4)	2.8(-4)	3.7(-4)	4.5(-4)	3.3(-6)
NIII	-	-	2.7(-9)	1.4(-7)	5.2(-8)	8.7(-8)	-	-	2.7(-8)	4.5(-6)	5.1(-8)	9.9(-8)	6.3(-6)	-
NIV	1.1(-7)	2.7(-6)	3.2(-5)	9.7(-5)	9.5(-5)	9.6(-5)	1.0(-6)	1.6(-5)	9.1(-5)	9.3(-5)	9.4(-5)	9.7(-5)	9.1(-5)	1.1(-5)
NV	3.9(-5)	9.4(-5)	6.6(-5)	7.6(-7)	2.9(-6)	1.2(-6)	9.0(-5)	8.1(-5)	6.3(-6)	1.9(-8)	3.3(-6)	1.1(-6)	5.1(-8)	8.7(-5)
OIV	6.5(-6)	1.3(-4)	6.5(-4)	8.2(-4)	8.3(-4)	8.2(-4)	4.6(-5)	4.8(-4)	8.3(-4)	4.8(-4)	8.3(-4)	8.3(-4)	6.3(-4)	3.8(-4)
OV	7.6(-4)	7.0(-4)	1.8(-4)	2.8(-7)	1.9(-6)	3.3(-7)	7.8(-4)	3.6(-4)	4.6(-6)	1.5(-8)	1.2(-6)	3.2(-7)	6.2(-8)	4.5(-4)
OVI	6.6(-5)	4.6(-7)	2.7(-9)	-	-	-	4.7(-6)	1.9(-8)	-	-	-	-	-	7.4(-8)
SiIV	-	-	1.5(-9)	3.1(-8)	1.1(-8)	1.8(-8)	-	-	5.8(-9)	3.3(-7)	1.1(-8)	2.0(-8)	1.7(-6)	-
SiV	3.2(-5)	3.2(-5)	3.2(-5)	3.2(-5)	3.2(-5)	3.2(-5)	3.2(-5)	3.2(-5)	3.2(-5)	3.1(-5)	3.2(-5)	3.2(-5)	3.0(-5)	3.2(-5)
PV	-	1.2(-9)	9.5(-9)	1.7(-7)	1.1(-7)	1.5(-7)	-	4.4(-9)	7.4(-8)	2.1(-7)	1.0(-7)	1.5(-7)	2.0(-7)	2.3(-9)
PVI	2.2(-7)	2.2(-7)	2.2(-7)	5.1(-8)	1.1(-7)	7.8(-8)	2.2(-7)	2.2(-7)	1.5(-7)	1.0(-9)	1.2(-7)	7.1(-8)	-	2.2(-7)
SIV	-	-	-	3.4(-8)	9.5(-9)	1.9(-8)	-	-	3.9(-9)	1.1(-6)	8.7(-9)	2.2(-8)	3.1(-6)	-
SV	-	7.1(-8)	1.1(-6)	1.4(-5)	1.2(-5)	1.4(-5)	1.2(-8)	5.5(-7)	9.4(-6)	1.5(-5)	1.1(-5)	1.4(-5)	1.3(-5)	2.8(-7)
SVI	1.5(-6)	1.3(-5)	1.5(-5)	1.7(-6)	3.9(-6)	2.3(-6)	8.1(-6)	1.5(-5)	6.4(-6)	1.7(-8)	4.8(-6)	2.1(-6)	5.2(-8)	1.5(-5)

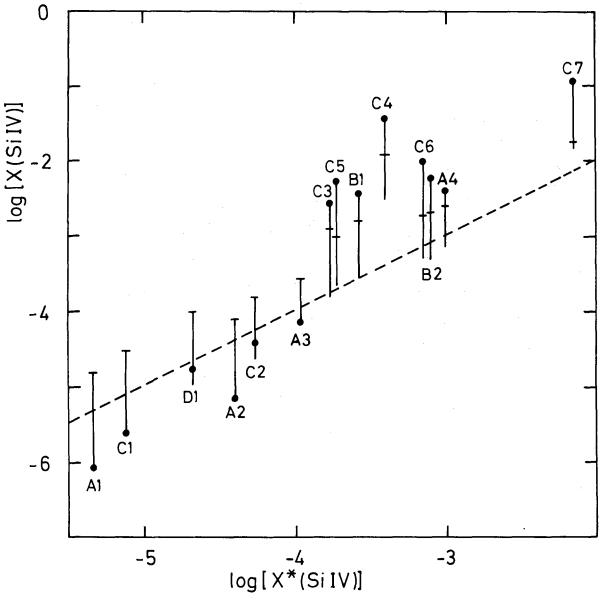

Fig. 7a. Correct calculated ionization fraction of Si IV versus the approximate ionization fraction obtained by recombination theory with geometrically diluted photospheric radiation. The vertical bars show the whole range of the radius dependent calculated values. Marked are the values at the sonic point (horizontal bars), and in the outermost part of the wind (circles). Si IV rates are shown for wind models of the tracks of initial mass 120 (A), 85 (B), 60 (C) and 40 (D) $M_\odot$ (for a detailed discussion see text)

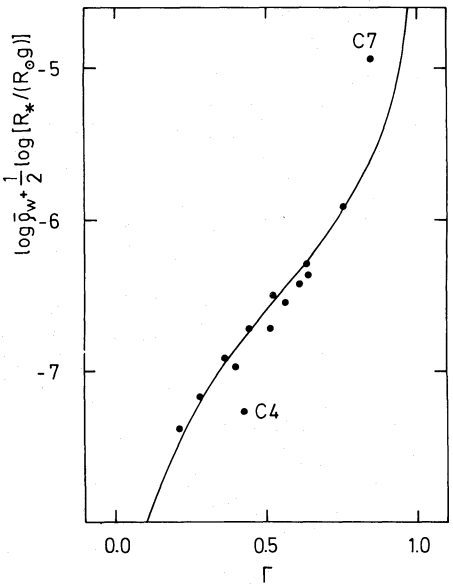

Fig. 7b. $\mathrm{Log}\,(\bar{\rho}_w(R_*/(R_\odot g))^{1/2}$ as a function of Γ, the ratio of luminosity divided by Eddington luminosity for the models of Table 1 and 3. The fully drawn curve is the relation of Eq. (4) for $\alpha = 0.6$ and a proportionality constant of $3.48\,10^{-7}$

X(Si IV) decreases with $T_{\rm eff}$ because of stronger ionization and increases with $\bar{\rho}_{\rm w}$ because of stronger recombination. For constant $T_{\rm eff}$ we obtain the luminosity effect because the wind density increases if we go vertically in the HR-diagram from the main sequence towards the Eddington-limit (see Table 3). This increase of $\bar{\rho}_{\rm w}$ with decreasing Γ is inherent in radiation driven wind theory. Since the mass-loss rates scale with $\dot{M} \approx L^{1/\alpha}(M(1-\Gamma))^{1-1/\alpha}$ and v_∞ is proportional to $v_{\rm esc} = (2GM(1-\Gamma)/R)^{1/2}$ we obtain

$$\bar{\rho}_{\rm w} \approx \left(\frac{g}{R}\right)^{1/2} \frac{\Gamma^{1/\alpha}}{(1-\Gamma)^{(1/\alpha - 1/2)}} \tag{4}$$

(Fig. 7b demonstrates that this proportionality is in most cases a reasonable description for the results of the detailed wind calculations). The luminosity dependence of the Si IV lines thus mainly reflects the increasing strengths of radiation driven winds with decreasing distance from the Eddington-limit.

3.2.2. An interpretation of the luminosity dependence of the O VI line

In view of the explanation of the Si IV luminosity effect it is somewhat surprising that the theoretical O VI line also exhibits a luminosity dependence (see Sect. 3.1), as shown by the fact that models A3, C2 show stronger wind components than less luminous, but slightly hotter models (D1), see Fig. 6a. At a first glance this seems to be in contradiction with the mechanism just described, where an increase in $\bar{\rho}_{\rm w}$ favours recombination and thus lower ionization stages, since here $\bar{\rho}_{\rm w}$ actually increases from model D1 to model C2 to A3 (see Table 3). We would expect, therefore, that the model with the highest $T_{\rm eff}$ and the lowest $\bar{\rho}_{\rm w}$ (i.e. model D1) should show the strongest O VI wind component. Fig. 6a clearly shows the opposite behaviour. To understand this result it is necessary to consider that the physical situations for oxygen and for silicon are not comparable, since Si IV is ionised by photospheric radiation, whereas O VI is produced by photons shortwards of the He II edge where the continuum is optically thick in the wind (see Pauldrach, 1987). In terms of the production of O VI, this means that an increase in the mean density leads not only to a larger recombination rate but also to a larger optical depth scale (τ_ν) in the frequency range of the O V ground state. Since an increase of the optical depth scale is in NLTE cases always connected with a decrease of the corresponding departure coefficient ($b = (n_{\rm O\,V,1}/n_{\rm O\,VI,1})/(n_{\rm O\,V,1}/n_{\rm O\,VI,1})^*$), an enhancement of the O V ground state ionisation rate is also induced by an increase in $\bar{\rho}_{\rm w}$. The latter conclusion is obvious from the following relation:

$$\frac{n_{\rm O\,VI,1}}{n_{\rm O\,V,1}} = \left(\frac{n_{\rm O\,VI,1}}{n_{\rm O\,V,1}}\right)^* \frac{1}{b} = \frac{R_{\rm O\,V,1;O\,VI,1}(J_\nu = B_\nu/b)}{R_{\rm O\,VI,1;O\,V,1}} \tag{5}$$

In the above equation $R_{\rm O\,V,1;O\,VI,1}$ is the ionisation rate from the O V ground state to the O VI ground state, where J_ν has been replaced by B_ν/b, which is correct for $\tau_\nu \gg 1$ and $R_{\rm O\,VI,1;O\,V,1}$ is the corresponding recombination rate. Hence, we see that it is not clear a priori whether an increase in $\bar{\rho}_{\rm w}$ leads to an enhancement of the O VI ionisation ratio due to an increase of the ionisation rate of O V – a consequence of the decrease in the departure coefficient – or to a reduction, due to an increase of the recombination rate, represented in Eq. (4) by the Saha Boltzmann factor. The situation is clarified by Fig. 6b, which shows the effects of both of the competing processes (note that the departure coefficients are obtained from the correct numerical treatment). As expected from the illustration of the O VI P-Cygni profiles (Fig. 6a), the O VI ratio is influenced most strongly by the reduction of the departure coefficient with $\bar{\rho}_{\rm w}$, at least up to velocities 10 times the sound velocity (note that $\bar{\rho}_{\rm w}$ increases systematically from model D1 to A3). Only in the outer part of the envelope does the situation change so that the number ratio of O VI decreases from model A3 to model D1, as might naively be supposed.

The similarity in the luminosity dependence of the Si IV and O VI lines demonstrates nicely that the completely different behaviour of the ionisation fractions, which at a first glance appears to be a contradiction, must be caused by strong NLTE effects.

3.2.3. Ionisation ratios

A quantitative representation of the results of the previous subsection is given in Table 5, where we show the ionisation ratios at a representative radius point for some important ionisation stages. The ionisation stages shown are those which give rise to resonance lines observed in the UV. The ratios are given in units of the H particle density at the radial point where $v = 0.4v_\infty$. It should be noticed that the ratios of subordinate ionisation stages, in particular C III, N III or Si IV, may vary strongly with position in the wind (see Paper III or above). Hence, an attempt to extrapolate these values may lead to meaningless results.

A comment is also necessary concerning the calculated ionisation ratios of C III and N III (see Table 5). Since the ground state ionisation edges of those ions are close to that of Si IV, they present similar optical depths to the ionising radiation. The ionisation ratios for these ions should therefore in most cases be also comparable to those obtained for Si IV, provided the recombination rates are similar. This is confirmed not only by the results shown in Table 5 but also by the ionisation fractions derived from observations for a sample of O stars by Olson and Castor (1981). This means that, although Pauldrach (1987, Paper III) had difficulties in reproducing the observed C III resonance line in the case of ζ Puppis, our present calculations yield population numbers for the C III and N III resonance lines which are at least in principle in agreement with the observations, and the deviations obtained in Paper III are probably due to the sensitivity of the trace ions on the radiation temperatures. This problem will be investigated in a forthcoming paper.

3.3. A comparison of dynamical properties with observations

In their comprehensive study of the wind properties of a sample of 205 O stars observed with IUE, Howarth and Prinja (1988) draw attention to a discrepancy between predictions of theoretical models obtained with the scaling laws given by Pauldrach et al. (1986) and observation. This discrepancy concerns the observed dependency of $v_\infty/v_{\rm esc}$ on the related stellar parameters $T_{\rm eff}$, R, L and $v_{\rm esc}$, which is not seen in the models of Pauldrach et al. (1986). In particular, the models yield $v_\infty/v_{\rm esc}$ ratios of nearly 2.0 for low temperatures (≈ 30 kK), low $v_{\rm esc}$ ($\approx 700\,{\rm km\,s^{-1}}$) and large radii ($\approx 30\,R_\odot$), whereas the observations show ratios between 2.0 and 4.5 in the same parameter range (see Howarth and Prinja, 1988, Fig. 10). Additionally, Howarth and Prinja have pointed out that the observed trends of increasing $v_\infty/v_{\rm esc}$ with increasing radius and of decreasing $v_\infty/v_{\rm esc}$ with increasing $v_{\rm esc}$ are also not obtained in the theoretical models.

To see whether this discrepancy remains with our new self-consistent calculations we have plotted $v_\infty/v_{\rm esc}$ against $\log T_{\rm eff}$,

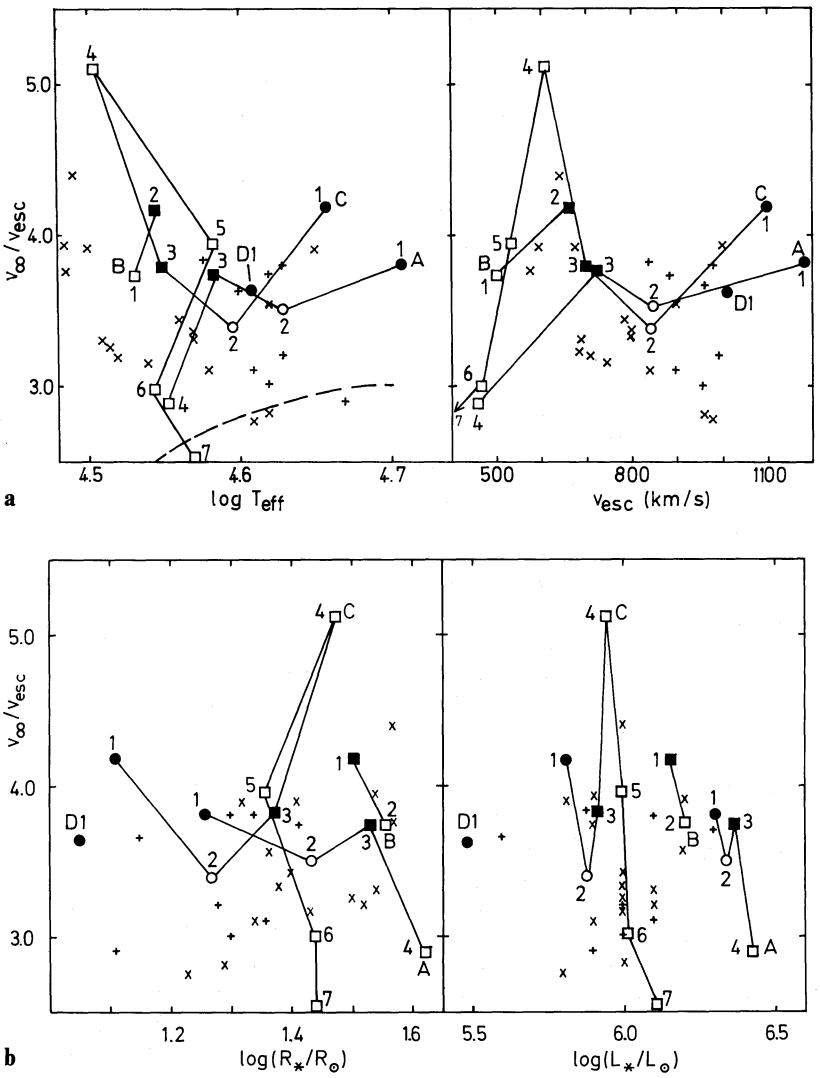

Fig. 8a and b. The ratio v_∞/v_{esc} as a function of stellar parameters. Shown are wind models along evolutionary tracks of initial masses 120 (A), 85 (B), 60 (C) and 40 (D) $M_\odot$, where filled circles correspond to early O dwarfs, open circles to early O giants, filled squares to bright O giants and open squares to middle O supergiants. Observed objects (from Howarth and Prinja, 1988), denoted by '×' (supergiants with $M/M_\odot \geq 52$) and by '+' (other luminosity classes with $M/M_\odot \geq 58$), are also shown for comparison. The dotted line in the v_∞/v_{esc} versus $\log T_{eff}$ diagram corresponds to previous theoretical predictions (discussion see text)

$\log(R/R_\odot)$, v_{esc} and $\log(L/L_\odot)$, in Fig. 8 for our model sequence of Table 3 and for the observed objects of Howarth and Prinja, where only supergiants with $M/M_\odot \geq 52$ and other luminosity class objects with $M/M_\odot \geq 58$ from the latter have been taken into account in view of the masses of our considered evolutionary tracks.

The result of this comparison is most encouraging, since it shows that the agreement between the currently most elaborate theory and the most comprehensive and detailed study of observations is striking. In particular the v_∞/v_{esc} vs. $\log T_{eff}$ diagram demonstrates that even the large observed variance in v_∞/v_{esc} for the supergiants is confirmed by our calculations at low temperatures. This large variance is caused by the back reaction of level population changes on the line force and the wind dynamics (for a description of this effect see Pauldrach, 1987). For instance, the largest value of v_∞/v_{esc}, which corresponds to model C4, is induced by a line force strongly influenced by the lower ionization stages (C III, N III, Si IV). They have more strong lines at the radiative flux maximum which increase the net radiative force. For model C4 this effect is caused by the strong UV blanketing of the corresponding Kurucz model (see Sect. 3.2), which decreases the radiative temperatures in relation to the effective temperature (see Table 4) and thus increases the population of the lower ionization stages and the terminal velocity in concert. It is also interesting to note that for both, the deviation from the approximate ionisation fraction of Si IV in Fig. 7 and the large v_∞/v_{esc} ratio, the photospheric line blanketing is responsible.

Additionally, it is obvious from Fig. 8 that the observed trends of increased v_∞/v_{esc} with increasing radius and of decreased v_∞/v_{esc} with increasing v_{esc}, is *not in contradiction* with our results. In Fig. 9 how the mass-loss rates develop along the tracks according to our calculations is illustrated. Also shown is the power-law dependence of $\dot{M}$ on $L/L_\odot$ and the inclined band of observed mass-loss rates derived recently by Howarth and Prinja (1988). Obviously, the calculated $\dot{M}$ are strongly correlated with the luminosity. However, the non-negligible back reaction of the level populations on the mass-loss rates (see models C2, 3, 4, 5) prevents a simple correlation between $\dot{M}$ and $L/L_\odot$ along the tracks. Particularly striking is the dramatic increase of $\dot{M}$ from models C5, C6 to model C7, which corresponds to the post RGB-stage close to the Eddington-limit, i.e. the domain of the Luminous Blue Variables. This jump in $\dot{M}$, which confirms the discontinuous behaviour of the mass-loss rates of LBVs like P-Cygni found by Pauldrach, Puls

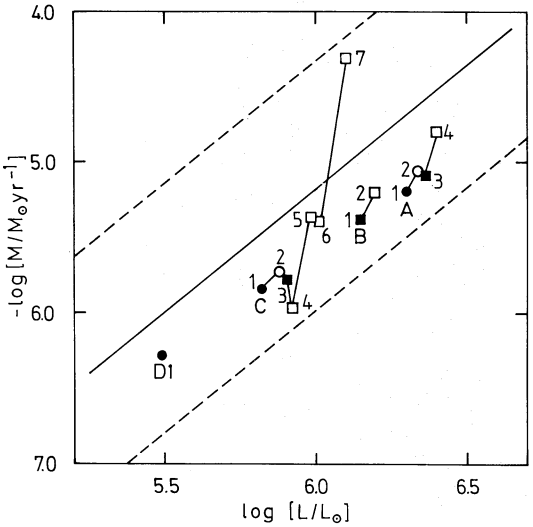

Fig. 9. Mass-loss rates as a function of luminosity. The wind models are denoted in the same way as in Fig. 8. Also shown is the power-law fit (fully drawn) and the inclined band (dashed) of observed mass-loss rates derived by Howarth and Prinja (1988)

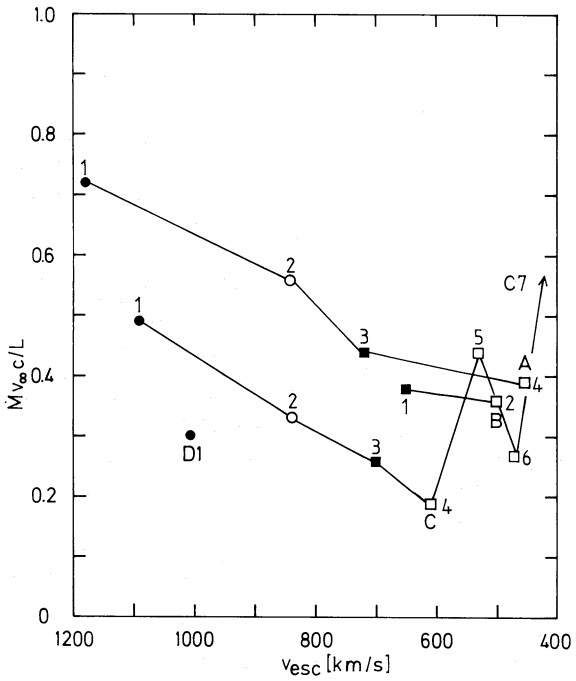

Fig. 10. The correlation of the wind efficiency ($\dot{M}v_\infty c/L$) with v_{esc} for the calculated objects (the symbols are explained in Figs. 8 and 9; note: the value for the post LBV model C7 is greater than one!) (for a discussion see text)

and Kudritzki (1988), possibly allows the wind properties of these extreme objects to be understood more precisely. The reason for this sudden increase in $\dot{M}$ is the strong influence of the Lyman continuum which suddenly becomes optically thick between models C6 and C7. This influences the wind ionization and, in turn, the radiative line acceleration (details are described by Pauldrach et al., 1988).

Another striking feature of Fig. 9 is that nearly all of our calculated mass-loss rates lie below the mean observed power-law found by Howarth and Prinja (1988). Besides the possibility that our calculations are affected by systematic errors, it should be emphasized that the normalising constant of the power-law depends entirely on radio mass-loss observations of supergiants (also noted by Howarth and Prinja), for which – in particular for the objects with large $\dot{M}$ (upper part of the diagram) – only uncertain upper limits are available (see Howarth and Prinja, 1988). Thus, it is most likely that the normalising constant of the power law fit has been overestimated.

We now briefly discuss another essential characteristic of stellar winds, the wind efficiency – the ratio of wind momentum to radiative momentum – $\dot{M}v_\infty c/L$. Figure 10 displays the relation of the wind efficiency versus the escape velocity for the individual tracks. As $\dot{M}$ is proportional to the luminosity with a power law index differing not too much from 1.10 (see Fig. 9) and v_∞ is proportional to the escape velocity, it is not astonishing that the wind efficiency is fairly well correlated with v_{esc} for each track. Due to the jump in $\dot{M}$ this correlation does not exist of course for the pre and post LBV objects. Instead, a dramatic increase in the wind efficiency ($\dot{M}v_\infty c/L > 1$) was found for the post LBV model (C7). For a detailed comparison, this model obviously requires the inclusion of multiple scattering effects (for details see Puls, 1987). A comparison of low mass objects with more massive objects of the same luminosity class is also shown in Fig. 10. We see that significantly higher wind efficiencies are obtained for the latter. Moreover, Fig. 10 shows a pronounced decrease of $\dot{M}v_\infty c/L$ from main sequence stars to supergiants. This slope indicates that a decreasing distance from the Eddington-limit is not sufficient to guarantee a large wind efficiency, a large value of $\log g$, which leads to an enhanced v_{esc}, is also necessary.

4. Conclusions and future work

In a systematic study, based on wind models computed along evolutionary tracks, we have shown that our calculations reproduce the observed changes of spectral morphology as a function of spectral type and luminosity class. This is demonstrated by the behaviour of the resonance lines of Si IV, C IV, N V and a subordinate line of N IV in a "semi-quantitative" sense. After a phase of calibration by *detailed quantitative star by star spectral analysis* of standards, our results will make it possible to use the ultraviolet wind spectra of O stars for direct luminosity determination. However, the present work is of course only a first step. Our treatment requires some refinement before the theory can really be used for detailed quantitative spectral analyses. In particular, the application of the LTE blanketed photospheric model atmospheres by Kurucz (1979) in the optically thin frequency part of the wind is a source of uncertainty, especially as the photospheric UV blanketing was shown to be important for the significant shift to the Si IV ionization stage of supergiants.

Another important consequence of our calculations is that O VI P-Cygni structures can be produced in cool wind models up to O7 bright giants, whereas for all cooler supergiants the amount of O VI was insufficient to produce P- Cygni profiles. Despite the fact that this result is not completely in agreement with observations (see Snow and Jenkins, 1977; Olson and Castor, 1981) it is most encouraging, since it shows that the stellar UV radiation field is dominated by the detected diffuse X-ray

radiation field (see Long and White, 1980; Cassinelli and Swank, 1983) only in very late O stars and, hence, Auger ionization due to X-rays, which has been neglected in our calculations, might not have too great an influence on the statistical equilibrium calculations. However, a more refined theory, in which photospheric and wind NLTE blanketing is taken into account the energy balance is treated self-consistently and precise atomic data are used, is necessary in order to obtain quantitative results (this work is under way in our group).

With regard to the dynamical properties it was shown that the discrepancy between the predictions of preceding theoretical models (Pauldrach et al., 1986) and the observed dependency of v_∞/v_{esc} on stellar parameters described by Howarth and Prinja (1988) has been resolved. In addition, agreement has been found between the calculated and observed mass loss rates and the discontinuous behavior of the mass-loss rates of LBVs has been confirmed. Finally, a strong dependency on mass, a pronounced decrease from main sequence stars to supergiants and a dramatic increase towards LBVs was found for the wind efficiencies $\dot{M}v_\infty c/L$. We should like to emphasize that detailed star by star spectral analyses of course require the inclusion of multiple scattering effects as outlined by Puls (1987).

From these results we conclude as usual that the concept of radiation driven cool winds seems to be the right way to describe quantitatively the rapidly expanding envelopes of hot stars.

Acknowledgements. We wish to thank our colleague Dr. A. Herrero (Tenerife) for helpful discussions. We would also like to thank, as a sort of astrophysical obituary, Dr. D.C. Abbott for his fundamental work over the years in the field of stellar winds. It is indisputable that the break throughs in recent years in this subject are to a large extent due to him. It is with deep regret that we note his departure from astrophysical research because of administrative ignorance. Finally, we also thank the referee, Dr. J. Castor for his useful comments. This work was supported by the DFG under grant Ku 474/11-3.

References

Abbott, D.C.: 1978, *Astrophys. J.* **225**, 893
Abbott, D.C.: 1979, IAU Symp. 83, p. 237, eds. P.S. Conti, C.W.H. de Loore
Abbott, D.C.: 1982, *Astrophys. J.* **259**, 282
Abbott, D.C., Hummer, D.G.: 1985, *Astrophys. J.* **294**, 286
Abbott, D.C., Lucy, L.B.: 1985, *Astrophys. J.* **288**, 679
Baade, D., Lucy, L.B.: 1987, *Astron. Astrophys.* **178**, 213
Cassinelli, J.P., Swank, J.H.: 1983, *Astrophys. J.* **271**, 681
Castor, J., Abbott, D.C., Klein, R.: 1975, *Astrophys. J.* **195**, 157
De Jager, C., Nieuwenhuijzen, H., van der Hucht, K.A.: 1988, *Astron. Astrophys. Suppl.* **72**, 259
Drew, J., 1989: *Astrophys. J.* (in press)
Friend, D., Abbott, D.C.: 1986, *Astrophys. J.* **311**, 701
Gabler, R., Gabler, A., Kudritzki, R.P., Puls, J., Pauldrach, A.W.A.: 1989, *Astron. Astrophys.*, (in press)
Garmany, C.D., Olson, G.L., Conti, P.S., van Steenberg, M.E.: 1981, *Astrophys. J.* **250**, 660
Howarth, J.D., Prinja, R.K.: 1989, *Astrophys. J. Suppl.* **69**, 527
Kudritzki, R.P., Simon, K.P., Hamann, W.R.: 1983, *Astron. Astrophys.* **118**, 245
Kudritzki, R.P., Hummer, D.G.: 1986, Proc. IAU Symp. 116, eds. C. Loore et al., p. 3
Kudritzki, R.P., Groth, H.G., Butler, K., Husfeld, D., Becker, S., Eber, F., Fitzpatrick, E.: 1987b, Proc. ESO Workshop *SN 1987a*, ed. I.J. Danziger, p. 37
Kudritzki, R.P., Pauldrach, A.W.A., Puls, J.: 1987a, *Astron. Astrophys.* **173**, 293
Kudritzki, R.P., Pauldrach, A.W.A., Puls, J., Abbott, D.C.: 1989, *Astron. Astrophys.* **219**, 205
Kudritzki, R.P.: 1988, 18th Advanced Course, Swiss Society of Astronomy and Astrophysics, Leysin, March 1988
Kudritzki, R.P., Gabler, A., Gabler, R., Groth, H.G., Pauldrach, A.W.A., Puls, J.: 1988, Proc. IAU Colloquium No. 113 *Physics of Luminous Blue Variables*
Lamers, H.J.G.L.M., Waters, L.B., Wesselius, P.R.: 1984, *Astron. Astrophys.* **134**, L17
Long, K.S., White, R.L.: 1980, *Astrophys. J. Letters* **239**, L65
Lucy, L.B., Solomon, P.: 1970, *Astrophys. J.* **159**, 879
Maeder, A., Meynet, G.: 1987, *Astron. Astrophys.* **182**, 243
Olson, G.L., Castor, J.: 1981, *Astrophys. J.* **244**, 179
Pauldrach, A.W.A., Puls, J., Hummer, D.G., Kudritzki, R.P.: 1985, *Astron. Astrophys.* **148**, L1
Pauldrach, A.W.A., Puls, J., Kudritzki, R.P.: 1986, *Astron. Astrophys.* **164**, 86
Pauldrach, A.W.A.: 1987, *Astron. Astrophys.* **183**, 295
Pauldrach, A.W.A., Herrero, A.: 1988, *Astron. Astrophys.* **199**, 262
Pauldrach, A.W.A., Kudritzki, R.P., Gabler, R., Wagner, A.: 1988a, Proc. 2nd Torino Workshop on Mass Outflow from Stars and Galactic Nuclei, eds. L. Bianchi, R. Gilmozzi, Reidel, Dordrecht, p. 63
Pauldrach, A.W.A., Puls, J., Kudritzki, R. P., Méndez, R., Heap, S.: 1988b, *Astron. Astrophys.* **207**, 123
Pauldrach, A.W.A., Puls, J., Kudritzki, R.P.: 1988, Proc. IAU Colloquium No. 113 *Physics of Luminous Blue Variables*
Puls, J.: 1987, *Astron. Astrophys.* **184**, 227
Schönberner, D., Herrero, A., Becker, S., Eber, F., Bulter, K., Kudritzki, R.P., Simon, K.P.: 1988, *Astron. Astrophys.* **197**, 209
Simon, K.P., Jonas, G., Kudritzki, R.P., Rahe J.: 1983, *Astron. Astrophys.* **125**, 34
Snow, T.P., Jenkins, E.B.: 1977, *Astrophys. J. Suppl.* **33**, 269
Voels, S.A., Hummer, D.G., Abbott, D.C., Bohannan, B.: 1989, *Astrophys. J.* **340**, 1073
Walborn, N.R., Panek, R.J.: 1984a, *Astrophys. J.* **280**, L27
Walborn, N.R., Panek, R.J.: 1984b, *Astrophys. J.* **286**, 718
Walborn, N.R., Panek, R.J.: 1985, *Astrophys. J.* **291**, 806
Walborn, N.R., Nichols-Bohlin, J.: 1987, *Publ. Astron. Soc. Pac.* **99**, 40
Walborn, N.R., Nichols-Bohlin, J., Panek, R.J.: 1985, *IUE Atlas of O-Type Spectra from 1200 to 1900 A*, NASA Reference Publication 1155